Vibration Characteristics and Condition Monitoring of Internal Radial Clearance within a Ball Bearing in a Gear-shaft-bearing system

Minmin Xu [a], Yaoyao Han [a], Xiuquan Sun [b], Yimin Shao [a]*, Fengshou Gu [b] and Andrew D. Ball [b]

[a] *State Key Laboratory of Mechanical Transmission, Chongqing University, Chongqing 400044, China.*

[b] *Centre for Efficiency and Performance Engineering, University of Huddersfield, Huddersfield HD1 3DH, UK.*

Abstract: Internal radial clearance is a key factor influencing bearing fatigue life. Moreover, bearings inevitably suffer from various wears and tears, which result in gradual increase of clearance and shorten bearing life. Monitoring bearing clearance changes using vibration can effectively indicate the bearing wear and provide good leading time to perform maintenances. Previous studies show that vibration at ball pass frequency on outer race (BPFO) can be based for clearance monitoring. However, such clearance induced vibration has not been well understood, especially under complicated dynamic interactions such as in a gearbox system. To fill this gap, this paper presents a nonlinear gear-shaft-bearing-housing vibration model with fourteen degree of freedom (DOF) to investigate the vibration responses under the dynamic gear meshing force and progressively changed radial clearances at first. Then, the model was verified through a two-stage spur gearbox. Furthermore, bearing characteristics with different radial clearances under the influence of gear are revealed and indicator based on modulation signal bispectrum-sideband estimator (MSB-SE) was proposed. Finally, vibration data from a run-to-failure gearbox test rig was utilized to verify the effectiveness of the MSB-SE indicator for bearing clearances monitoring. Simulation results show that BPFO is modulated on gear meshing frequency (GMF) and BPFO amplitude from envelope spectrum increases with bearing clearances under the influence of gear meshing. Indicator based on MSB-SE, possessing the capability of purifying the interferences of gear meshing and strong noises, is effective to capture the variance of bearing clearances. The experiment based on a run-to-failure gearbox test rig provided evidence for the effectiveness of the proposed indicator, which is more accurate than BPFO amplitude from conventional envelope analysis and time-domain indicators, such as RMS and kurtosis. These findings are of significance for bearing fault diagnosis and maintenance.

Keywords: Rolling element bearing, Internal radial clearance, Gear-shaft-bearing-housing system, Modulation signal bispectrum-sideband estimator, Gearbox condition monitoring

1. Introduction

Rolling element bearings and gear are key components in rotating machinery, especially in a gearbox, which realize the transmission of power and motion and is widely used in many major fields of industrial production, such as machine tools, vehicles and wind turbines [1][2][3][4]. Complex working environments can easily reduce the reliability of bearings and induce various faults on bearings, resulting in unscheduled maintenance and downtime [5][6]. For example, in wind turbine system, over 50% of faults in gearboxes were related to bearings [7] and abrasive wear is the most common [8]. Thus, accurate condition monitoring of bearings is of great significance to the actual production.

Internal radial clearance is the play within a ball bearing. It is the geometrical clearance between the inner ring, outer ring and ball. Different from bearings with tapered roller elements, in which the clearance can be adjusted at the time of assembly, the clearance of a ball bearing is determined after design and construction. Thus, it is a fundamental factor in bearing selection before the machine running due to its direct effect on bearing rotating life, temperature and vibration [9]. Besides, it is well deemed that bearings undergo various wear and tear, which are the key type of bearing invalidation during their lifetimes and reduce bearing service time by about 30% [10]. However, wear during the bearing lifetime is difficult to measure because of the compact structure with a narrow space. Debris is feasible for measuring wear loss, but it needs extra particular equipment [11]. Fortunately, wear on bearings will leads to large clearances and high vibrations [12][13]. Consequently, considering the significant influence of bearing clearance on bearing load distribution and fatigue life [14][15], it is urgent to study the mechanism and monitoring of bearing internal clearances from vibration signals.

To reveal the mechanism of clearances, literature can be found focusing on modeling bearing vibration responses taking into account the effect of bearing clearance [16][17][18][19]. However, from above studies, it finds that bearing clearances usually regarded as a constant in different models, which did not correspond to the increasing bearing clearance under different kinds of wear and tear during its lifetime. Besides, a comprehensive cognition of clearance can be formed when focusing on

different levels of bearing clearances on vibrational responses, which will be benefit to account for various vibration phenomena and monitor bearing clearances. On this aspect, Oswald [10] utilized empirical equations to study the bearing load distribution and fatigue life of ball and roller bearings with radical load considering four levels of internal radial clearances. Recently, Rehab et al. [13] investigated the diagnostic features under two group bearing clearances through model-based method with presenting a nonlinear dynamic shaft-bearing-housing model and point out the difference on characteristic frequencies of bearings with local defect. More recently, in [20], the authors studied the bearing vibration characteristics when taking into account continuously changing bearing clearances from 0 to 100μm and different working conditions through a six-degree-of-freedom (DOF) dynamic model. It found that ball pass frequency of outer race (BPFO) is conspicuous through the envelope spectrum for ball bearing before obvious local defect on raceways. The above studies, especially through model-based method, were meaningful explorations on bearing clearances, but the mechanism seems like insufficient to match with the complex working conditions and wide applications of bearings, especially in a gear-shaft-bearing-housing system, a typical structure in gearbox. Under this case, the motion of bearing and gear are coupled together dynamically, combined with the complicated modulation and noise effect, it is difficult to distinguish and diagnose the fault of bearing and gear. Even it is more meaningful to reveal the ambiguous interaction between them, the mechanism study in this field remains rare.

In real application, bearing and gear usually work together and both of them are key components in a gearbox, which is widely used in mechanical transmission. To study the dynamic behaviors of bearings or (and) gears in a gear-shaft-bearing system, some relevant works could be found from literature. Sawalhi and Randall [21][22] presented a vibration model for a gearbox test rig and investigated the interactions between gear and bearing in the presence of bearing localized faults, including inner race, outer race and rolling elements defects. Zeng et al. [23] established a dynamic model of a gear-shaft-housing system by finite element method to investigate the vibration responses of different points on the gearbox and pointed out that the vibration increases with the gear meshing stiffness. Hu et al. [24] developed a finite element node dynamic model of a high-speed gear-rotor-bearing system considering the time-varying mesh stiffness, backlash, gyroscopic effect and transmission error excitation. Xiao et al. [25] explored the vibration transmission characteristics and energy dissipation through an eight-degree-of-freedom (DOF) dynamic model of the gear-shaft-bearing-housing system through the multiple transmitting interfaces under the impulsive force due to the gear fault. Fernandez et al. [26] proposed an enhanced model of gear transmission dynamics for condition monitoring considering the effect of bearing clearances. Chen et al. [27] investigated the characteristics of the geared rotor-bearing system taking into account gear meshing, shaft and oil-film bearing. It finds that above studies mainly focus on gear dynamics through considering the influences of bearing in a gear-bearing system, few of them investigated the effect of dynamic gear meshing force on bearing vibration characteristics, especially on bearing clearances before distinct localized defects.

On the other hand, to monitor the bearing clearances, encouraged by tribology-focused techniques on diagnosing bearing wear through measured condition monitoring data [12][28], efforts can be found in previous studies. Zmarzły [29] evaluated the vibration level affected by bearing radial clearance through experiment and pointed out that bearing clearances has an effect on the frequency spectrum components in medium frequency band. Georgiadis et al. [30] used spectral kurtosis to indicate bearing clearance changes through the measured vibration data under different rotating speed. Yakout et al. [15] studied the variance of bearing damping characteristics and natural modes under different radial clearances through experimental tests. However, the simple indicators from frequency domain are easily affected by other joint components through modulation and are also contaminated by background noise, which bring many difficulties for bearing clearances monitoring. In [31], kurtosis, recurrences and neural networks were adopted to measure changes of the bearing vibration level and signal structure under different clearances. In [20], the authors investigated the bearing vibration responses under different clearances and working conditions through model-based method and found that both RMS and spectral centroid increase with the radial clearance in general but some local fluctuations. Through the verification of simulation and tested signals, the spectral centroid shows better performance on monitor clearance. However, it is suitable for the simple bearing system, which is rare in real applications. But in real application, bearing usually work with other mechanical components, such as gears. Under such circumstances, modulation phenomenon happened duo to the nonlinear relationship among bearings, gears and other components with certain complexity. In addition, investigations show that when a gearbox is in good condition, due to a near normal distribution of the frequency amplitude on gear meshing frequency (GMF) and its harmonics, many time-domain monitoring indicators, such as variance and kurtosis, usually give a stable value close to zero [32]. Especially, for a gearbox operating under normal conditions, the vibration signature of the bearings is weak, and it is usually masked by the

vibrations from the meshing excitations [33]. Fortunately, investigations show that focusing on the modulation between the GMF and the associated shaft frequency can indicate tooth wear during the long-time operation [34][35][36]. It seems that study on effect of gear meshing on bearing from mechanism could provide more useful information for bearing clearance monitoring, which is a promising work. More recently, Wang et al. [37] attempted to monitor the change of bearing clearance online based on modulation signal bispectrum (MSB) and Gini-index, which is a comparatively rough estimation on three shafts rather than precise assessment for each bearing.

Overall, literature can be found concentrated on bearing clearances and pointed out significant findings; three shortcomings were existed in these studies. The first one is lacking sufficient mechanism research, failed to consider the variances of clearances due to bearing wear and especially failed to reveal the influence of dynamic gear meshing force on bearing clearances in a gearbox. The second one can be attributed to incomplete vibration characteristics. Due to the insufficient mechanism study, it is still not revealed what characteristics the response will show in such a gear-shaft-bearing system, resulting in difficulties to realize the bearing clearance monitoring. The third shortcoming consists in insufficient reasonable monitoring indicators, which made it impossible for accurate monitoring of bearing clearance online. All these deficiencies lead to incomplete understanding of bearing clearance and result in disadvantage for bearing detection and maintenance.

Thus, to bridge the gap, this paper devoted to study on bearing clearance taking into account the influence of gear dynamics through a nonlinear gear-shaft-bearing-housing vibration model, which is proposed to reveal the mechanism between bearing and gear and investigate the vibration characteristics and indicators for bearing clearances monitoring. Firstly, a fourteen-DOF gear-shaft-bearing-housing dynamic model, including nonlinearity of radial clearance and dynamic gear meshing force, is established on the basis of kinematics analysis. Then, a spur gearbox test was used to verify the rationality of the proposed vibration model. Furthermore, vibration characteristics at a gradually extended range of radial clearance were expounded and clearance monitoring indicators were proposed based on MSB-SE. Finally, the effectiveness of MSB-SE indicator was verified through a run-to-failure two-stage gearbox test rig.

2. Numerical Model of Bearing Clearances in a Gearbox

2.1 Gear-shaft-bearing-housing Model

In previous works, vibration responses of a single bearing under different radial clearances and constant external load were expounded through model based method, ignoring the influence of dynamic load. Thus, in this paper, to reveal the bearing vibration responses under various radial clearances with the influence of gear dynamics, aiming to explore the interaction between bearings and gears on spectrum from kinetic analysis, a lumped gear-shaft-bearing-housing vibration model is developed with fourteen DOFs, as is shown in **Fig. 1**. The model consists of a pair of gear, two shafts and four bearings. The detailed bearing and the gear vibration model is shown in **Fig. 2** and **Fig. 3**, respectively.

Besides, wear is one of the major failure modes happened in gear transmission system and progressive material loss during the wear process could lead to occurrence of other failures, such as pitting, spalling, which affects the fatigue life of gear. Thus, it is noted that, to consider the complexity of a gear-shaft-bearing-housing system, both normal gear and gear with spalling defect were included in the proposed model as different cases to mimic real working condition. Especially, there is only one obvious spalling on gear surface and the increase of spalling size was set as the increase of width in this study.

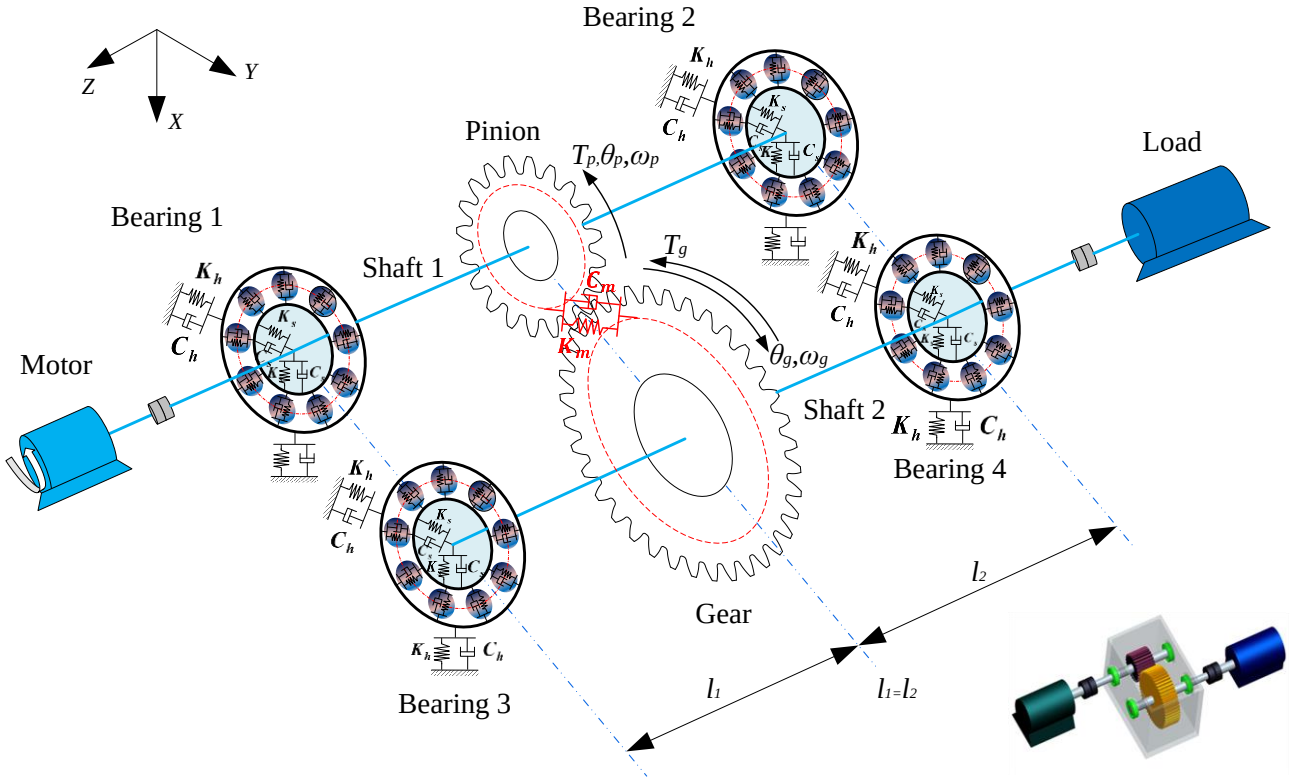

Fig. 1. Schematic diagram of a gear-shaft-bearing-housing vibration system

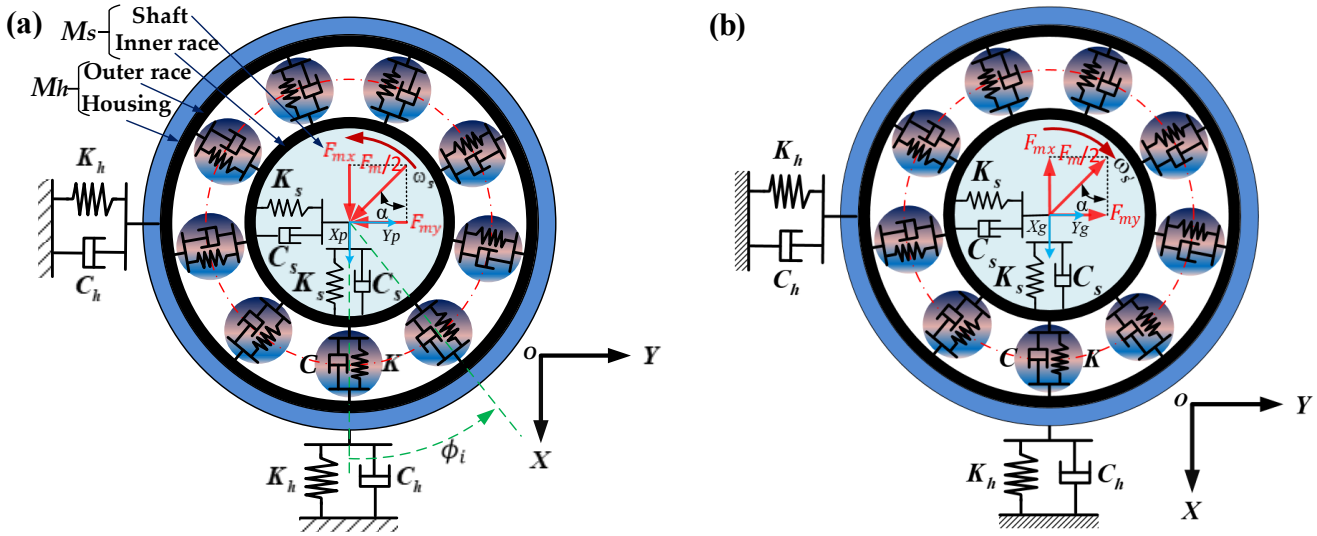

Fig. 2. Schematic diagram of bearing vibration model in the system: **(a)** bearing 1,2 and **(b)** bearing 3,4

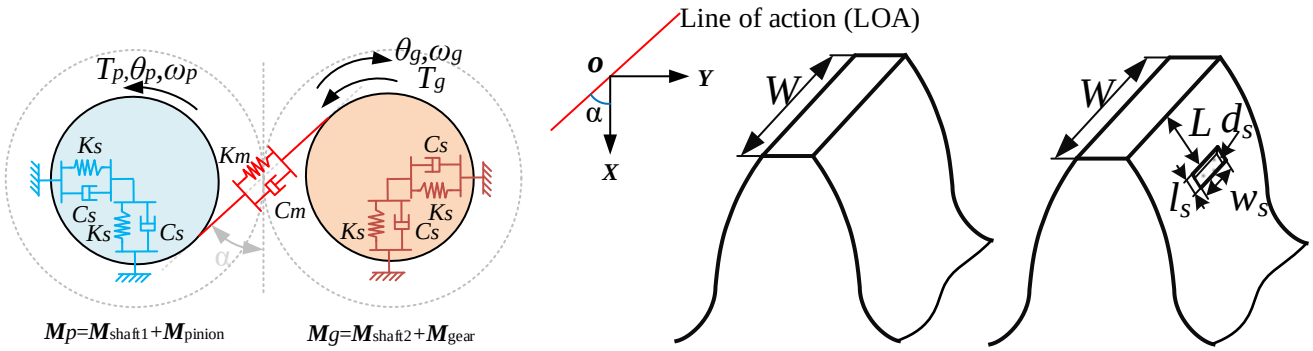

Fig. 3. Schematic diagram of a gear vibration model in the system

The gear-shaft-bearing-housing vibration model can be presented in Eq. (1)–(14). For the bearing part, M denotes the

mass of each component in bearing system, while the subscript s and h stands for shaft and housing, respectively. K and C means stiffness and damping coefficients, respectively. Particularly, K_{sh} and C_{sh} represent the stiffness and damping between raceways and rolling elements. Besides, δ_{ij} and v_{ij} means the nonlinear deformation and nonlinear velocity of the i^{th} ball, respectively; ϕ_{ij} represents the angle position of the i^{th} ball; N_b denotes the number of rolling elements. X_{ij}, $\dot{X}_{ij}$ and $\ddot{X}_{ij}$ stands for the displacement/velocity/acceleration in x direction, while Y_{ij}, $\dot{Y}_{ij}$ and $\ddot{Y}_{ij}$ means the displacement/velocity/acceleration in y direction. The subscript $i = s,h$ for shaft and housing, while $j = 1,2$ means bearings on shaft 1 and shaft 2, respectively. For the gear part, M_i and J_i is the mass and moment of inertia of gears, respectively. T_i is the applied torque, $\ddot{\theta}_i$ represents angular acceleration, $X_i/\dot{X}_i/\ddot{X}_i$ stands for displacement/velocity/acceleration in x direction, $Y_i/\dot{Y}_i/\ddot{Y}_i$ is displacement/velocity/acceleration in y direction, M_{iN} means the normal mesh force moment, M_{if} is the friction force moment, N is the net contact force due to the elasticity, and the subscript $i = p,g$ for pinion and gear, respectively.

$$M_s\ddot{X}_{s1} + C_s(\dot{X}_p - \dot{X}_{s1}) + K_s(X_p - X_{s1}) + \sum_{i=1}^{N_b} K_{sh}[\delta_{i1}]^{3/2}\cos\phi_{i1} + \sum_{i=1}^{N_b} C_{sh}[v_{i1}]\cos\phi_{i1} = (F_m\cos\alpha)/2, \quad (1)$$

$$M_s\ddot{Y}_{s1} + C_s(\dot{Y}_p - \dot{Y}_{s1}) + K_s(Y_p - Y_{s1}) + \sum_{i=1}^{N_b} K_{sh}[\delta_{i1}]^{3/2}\sin\phi_{i1} + \sum_{i=1}^{N_b} C_{sh}[v_{i1}]sin\phi_{i1} = (-F_m\sin\alpha)/2, \quad (2)$$

$$M_h\ddot{X}_{h1} + C_h\dot{X}_{h1} + K_hX_{h1} - \sum_{i=1}^{N_b} K_{sh}[\delta_{i1}]^{3/2}\cos\phi_{i1} - \sum_{i=1}^{N_b} C_{sh}[v_{i1}]\cos\phi_{i1} = 0, \quad (3)$$

$$M_h\ddot{Y}_{h1} + C_h\dot{Y}_{h1} + K_hY_{h1} - \sum_{i=1}^{N_b} K_{sh}[\delta_{i1}]^{3/2}\sin\phi_{i1} - \sum_{i=1}^{N_b} C_{sh}[v_{i1}]\sin\phi_{i1} = 0, \quad (4)$$

$$M_s\ddot{X}_{s2} + C_s(\dot{X}_g - \dot{X}_{s2}) + K_s(X_g - X_{s2}) + \sum_{i=1}^{N_b} K_{sh}[\delta_{i2}]^{3/2}\cos\phi_{i2} + \sum_{i=1}^{N_b} C_{sh}[v_{i2}]cos\phi_{i2} = (-F_m\cos\alpha)/2, \quad (5)$$

$$M_s\ddot{Y}_{s2} + C_s(\dot{Y}_g - \dot{Y}_{s2}) + K_s(Y_g - Y_{s2}) + \sum_{i=1}^{N_b} K_{sh}[\delta_{i2}]^{3/2}\sin\phi_{i2} + \sum_{i=1}^{N_b} C_{sh}[v_{i2}]sin\phi_{i2} = (F_m\sin\alpha)/2, \quad (6)$$

$$M_h\ddot{X}_{h2} + C_h\dot{X}_{h2} + K_hX_{h2} - \sum_{i=1}^{N_b} K_{sh}[\delta_{i2}]^{3/2}\cos\phi_{i2} - \sum_{i=1}^{N_b} C_{sh}[v_{i2}]\cos\phi_{i2} = 0, \quad (7)$$

$$M_h\ddot{Y}_{h2} + C_h\dot{Y}_{h2} + K_hY_{h2} - \sum_{i=1}^{N_b} K_{sh}[\delta_{i2}]^{3/2}\sin\phi_{i2} - \sum_{i=1}^{N_b} C_{sh}[v_{i2}]\sin\phi_{i2} = 0, \quad (8)$$

$$J_p\ddot{\theta}_p = T_p - M_p \quad (9)$$

$$J_g\ddot{\theta}_g = T_g - M_g \quad (10)$$

$$M_p\ddot{X}_p = F_m\cos\alpha - K_s(X_p - X_{s1}) - C_s(\dot{X}_p - \dot{X}_{s1}) \quad (11)$$

$$M_g\ddot{X}_g = -F_m\cos\alpha - K_s(X_g - X_{s2}) - C_s(\dot{X}_g - \dot{X}_{s2}) \quad (12)$$

$$M_p\ddot{Y}_p = -F_m\sin\alpha - K_s(Y_p - Y_{s1}) - C_s(\dot{Y}_p - \dot{Y}_{s1}) \quad (13)$$

$$M_g\ddot{Y}_g = F_m\sin\alpha - K_s(Y_g - Y_{s2}) - C_s(\dot{Y}_g - \dot{Y}_{s2}) \quad (14)$$

As can be seen from the schematic diagrams and dynamics equations, the bearing and gear are coupled together through the motion of shaft and gear, shaft supporting stiffness and gear dynamic meshing force. Under this circumstance, gear meshing force will act as an external load on bearings with dynamic characteristics, which is different from a constant load on bearing vibration responses, while bearing motion influence gear meshing in turn. But to simplify the model, the developed vibration model was constructed on the basis of the following assumptions and considerations.

(1) In the whole system, the displacement, velocity and acceleration in axial direction (Z) were ignored, i.e., only vertical (X) and horizontal (Y) direction was taken into account.

(2) In the whole system, errors derived from geometry and assembly were ignored.

(3) The vibration system operates under sufficient lubrication and isothermal conditions, i.e., insufficient, abnormal lubrication and temperature are not considered.

(4) The shaft was rigid, and torsional deformation and deflection are ignored in this model. It means that the symmetrically placed baring 1 and bearing 2 have the same response, while bearing 3 and bearing 4 are the same.

(5) For the bearing, sliding and skidding between raceways and rolling elements are neglected, i.e., the motion among them is treated as pure rolling.

2.1.1 Bearing Deformation and Contact Stiffness

In the bearing vibration model, the deformation δ_i and velocity v_i for each element could be calculated by the displacement/velocity of the shaft, housing and the orbital angle of ball, as shown in Eq.(15) [13][38] and Eq.(16) [20]

$$\delta_i = \begin{cases} (X_s - X_h)\cos\phi_i + (Y_s - Y_h)\sin\phi_i - c/2 \times (1 - \cos\phi_i) & \delta_{bi} > 0, \\ 0 & \delta_{bi} \le 0, \end{cases} \quad (15)$$

$$v_i = \begin{cases} (\dot{X}_s - \dot{X}_h)\cos\phi_i + (\dot{X}_s - \dot{X}_h)\sin\phi_i & \delta_{bi} > 0, \\ 0 & \delta_{bi} \le 0. \end{cases} \tag{16}$$

where c denotes radial clearance.

The total comprehensive stiffness among the inner race, rolling element and outer race can be obtained through Hertz contact theory [14], which is given as

$$K_{sh} = \left[\frac{1}{(1/K_i)^{1/(3/2)} + (1/K_o)^{1/(3/2)}}\right]^{3/2} \tag{17}$$

where $K_{i,o}$ is the Hertz contact stiffness between the outer and inner raceways with the ball, respectively.

$$K_{i,o} = \frac{2\sqrt{2}\left(\frac{E}{1-\nu^2}\right)}{3(\sum\rho)^{1/2}}\left(\frac{1}{\delta^*}\right)^{3/2} \tag{18}$$

where E is Young's modulus, ν is Poisson's ratio, $\sum\rho$ is the curvature sum and δ^* is the dimensionless contact deflection.

The equivalent damping coefficient [39][40] between two raceways of the bearing can be obtained on the basis of the mass and stiffness of rolling element, as well as a damping ratio.

$$C_{sh} = 2\varsigma\sqrt{m_b \times K} \tag{19}$$

where ς is the damping ratio and m_b is the mass of each ball. It is noted that the damping of the shaft and housing are also calculated according to Eq. (19) with its corresponding mass and stiffness.

2.1.2 Gear Deformation and TVMS

In the gear vibration model, the time-varying mesh force can be calculated through the time varying mesh stiffness (TVMS) and damping, as shown in Eq.(20). The dynamic normal mesh force and friction force, as well as the moments, among the gear pair can be expressed as

$$F_m = K_m\delta_{pg} + C_m\nu_{pg} \tag{20}$$

$$M_p = F_m \times r_{bp} \tag{21}$$

$$M_g = F_m \times r_{bg} \tag{22}$$

where, K_m means the TVMS, C_m represents the mesh damping. The relative displacement δ_{pg} and velocity and v_{pg} can be given as

$$\delta_{pg} = \begin{cases} (X_g - X_p)cos\alpha + (Y_p - Y_g)sin\alpha + r_{bp}\theta_p + r_{bg}\theta_g & \delta_{pg} > 0, \\ 0 & \delta_{pg} \le 0, \end{cases} \tag{23}$$

$$v_{pg} = \begin{cases} (\dot{X}_g - \dot{X}_p)cos\alpha + (\dot{Y}_p - \dot{Y}_g)sin\alpha + r_{bp}\omega_p + r_{bg}\omega_g & \delta_{pg} > 0, \\ 0 & \delta_{pg} \le 0. \end{cases} \tag{24}$$

where α is the contact angle and r_{bi} is the base radius.

During the meshing process, the TVMS of the gear pair changes with the alternate mesh of single and double teeth. According to the beam deformation theory in material mechanics, based on the above gear tooth bending deformation, shear deformation, axial compression deformation, Hertz contact deformation and matrix deflection deformation, the meshing stiffness excitation of the gear pair can be obtained by, [1][3]

$$k(t) = \sum_{j=1}^{2} 1/\left[\frac{1}{K_{h,j}} + \sum_{i=p,g}\left(\frac{1}{K_{bi,j}} + \frac{1}{K_{si,j}} + \frac{1}{K_{ai,j}} + \frac{1}{K_{fi,j}}\right)\right] \tag{25}$$

where subscripts $j = 1,2$ stands for the first tooth gear pair and second gear pair. K_b, K_s, K_a, K_f and K_h denotes bending stiffness, shear stiffness and axial compression stiffness, Hertzian contact stiffness and the deflection stiffness, respectively, which can be obtained through energy method expressed as [41][42]

$$\frac{1}{K_b} = \int_0^d \frac{[(d-x)\cos\alpha_1 - h\sin\alpha_1]^2}{EI_x}dx,\ \frac{1}{K_s} = \int_0^d \frac{1.2\cos^2\alpha_1}{GA_x}dx,\ \frac{1}{K_a} = \int_0^d \frac{\sin^2\alpha_1}{EA_x}dx,\ \frac{1}{K_h} = \frac{4(1-\nu^2)}{\pi EL},\ K_f = \frac{F}{\delta_f} \tag{26}$$

where, E and G are the elastic modulus and shear modulus of the material respectively; I_x and A_x are respectively the moment of inertia and the area of the section at the point x from the action point of meshing force, ν is Poisson's ratio, L is the tooth width, F is the mesh force in the action line and δ_f is the fillet-foundation deflection.

2.2 Model Setup and Characteristic Frequencies

In the vibration model, bearing 6205 is adopted to investigate the effect of bearing clearance. The main geometry parameters and main physical properties were shown in **Table 1** and **Table 2**, respectively. Besides, the main physical properties of the gear pair and the gear spalling size are shown in **Table 3** and **Table 4**, respectively.

Table 1
Main geometry parameters of deep groove ball bearing 6205

Description	Notation	Value
Nominal bore diameter (mm)	d	25
Nominal outside diameter (mm)	D	52
Inner race diameter (mm)	d_i	30.60
Outer race diameter (mm)	d_o	46.40
Pitch diameter (mm)	d_m	46.96
Ball diameter (mm)	d_b	7.90
Number of rollers	N_b	9
Contact angle (˚)	α	0°
Original radial clearance (μm)	c	0, 20

Table 2
The main physical properties for bearing study

Description	Notation	Value
Mass of shaft (kg)	m_s	1.30
Mass of house (kg)	m_h	0.50
Mass of each ball (kg)	m_b	2.95×10^{-3}
Stiffness of shaft (N/m)	K_s	3.0×10^{8}
Stiffness of housing (N/m)	K_h	5.0×10^{8}
Damping of shaft	C_s	3949.68
Damping of housing	C_h	3162.28

Table 3
The main parameters of the gear pair

Parameters	Pinion	Gear
Module (mm)	3	3
Teeth number	25	53
Pressure angle (°)	20°	20°
Width (mm)	60	50
Moment of inertia (kg•m2)	1.37×10^{-3}	2.31×10^{-2}
Mass (kg)	1.56	5.85
Torque (Nm)	28.30 $(60/z_2 \times z_1)$	60 (set by the brake)
Driven speed (rpm)	1500	194.73
Poisson's ratio	0.3	0.3

Table 4
The main parameters of the gear spalling

Parameters of Spalling	Notation	Value
Length (mm)	l_s	2
Width (mm)	w_s	0,10,20,30,40
Depth (mm)	d_s	1
Distance to the gear top (mm)	L	1.8

2.3 Dynamic Response

The main characteristic frequencies of the bearing and the gear are shown in **Table 5** and **Table 6**.

Table 5
Characteristic frequencies of the gear

Characteristic Frequencies (1500 rpm)	Notation	Value
First-order Mesh frequency	$1 * f_m$	625
Second-order Mesh frequency	$2 * f_m$	1250
Third-order Mesh frequency	$3 * f_m$	1875

Table 6
Characteristic frequencies of the bearing

Characteristic Frequencies	Bearing on Shaft I (1500 rpm)	Bearing on Shaft II (1500/53×25=707.55 rpm)
Rotational frequency f_{r1}	25	11.79
BPFO (Hz)	89.42	42.18
BPFI (Hz)	135.58	63.95
Cage frequency	9.94	4.69
BSF	58.35	27.52

To show the influence of clearance on vibration based on the dynamic model, taking a typical working condition with the rotational speed of 1500rpm and torque of 60Nm as an example, when gear is normal, the waveform and FFT spectrum of bearing 1,2 with and clearances of 0μm and 20μm are shown in **Fig. 4**. From time domain, the waveform presents impulses with the period of $1/f_m$, while the amplitude of these impulses fluctuate with another period of 1/BPFO related to bearing. And a higher fluctuation happens when under a larger bearing clearance (20μm). From the FFT spectrum, it finds that GMF and its harmonics are key frequency components. Especially, the harmonics of the GMF in high frequency band have comparatively higher amplitudes due to the resonant frequency of shaft (about 2417.74Hz) and housing (about 5032.92Hz) in the vibration system. However, in real gearbox test, high frequency band usually weakened by transmission path and energy dissipation, while low frequency band shows much energy from the spectrum. Thus, considering the characteristics of the real test, this study focused on low frequency band. From **Fig. 4(c)**, sidebands of BPFO can be seen from both side of GMF and its harmonics. In addition, the sidebands are more distinct with clearance of 20μm than zero clearance. Based on the sideband analysis, envelope spectrum is utilized to reveal the modulation components, as shown in **Fig. 5**, which shows higher amplitude on BPFO under lager clearance. Besides, the similar results can be found when spalling on gears ($w_s = 20mm$). It is noted that envelope spectrum was carried out on the narrow frequency band between 0Hz and 1875Hz ($3.5 \times f_m$), which covering the first three GMF harmonics. If there is no special description, the envelope spectra are operated on this frequency band in this study.

To show the influence of gear on the system, vibration responses under normal gear and spalling gear ($w_s = 40mm$) are depicted in **Fig. 6**, while clearance is set as 20μm. It can also find that the waveform presents periodic impulses with the frequency of GMF. In addition, when spalling occurs on gear surfaces, more obvious impulses can be discovered with the frequency of f_{r1}, which can be found in envelope spectrum and is higher than BPFO of bearing.

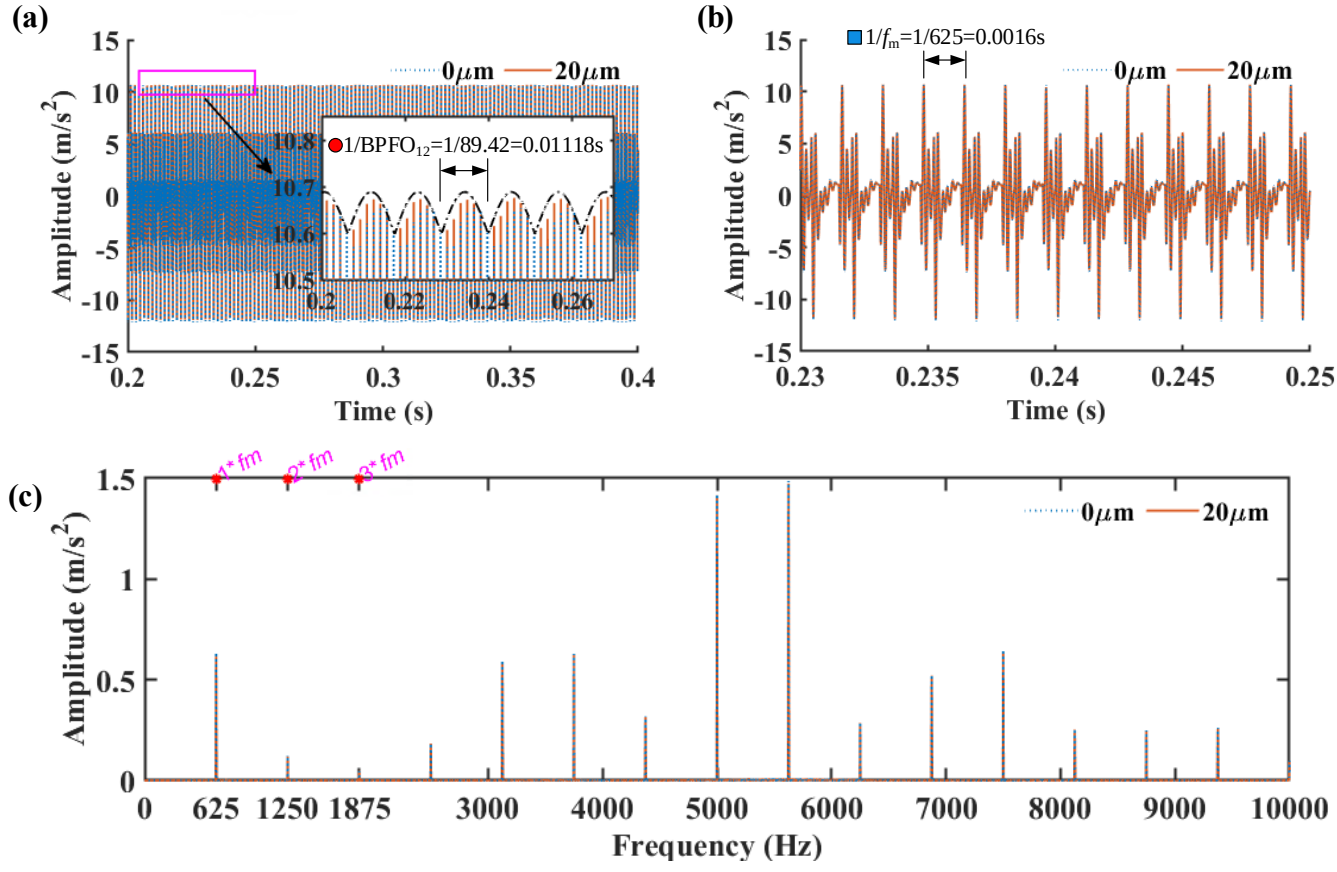

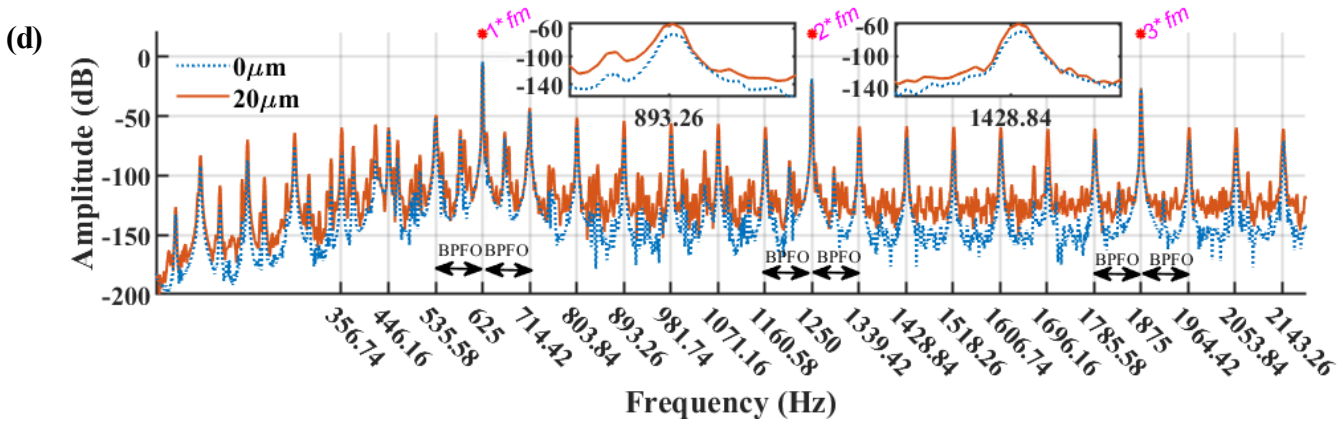

Fig. 4. Numerical simulation results of bearing 1,2 on vertical direction: **(a, b)** waveform, **(c)** FFT spectrum and **(d)** low frequency band of first three harmonics of GMF

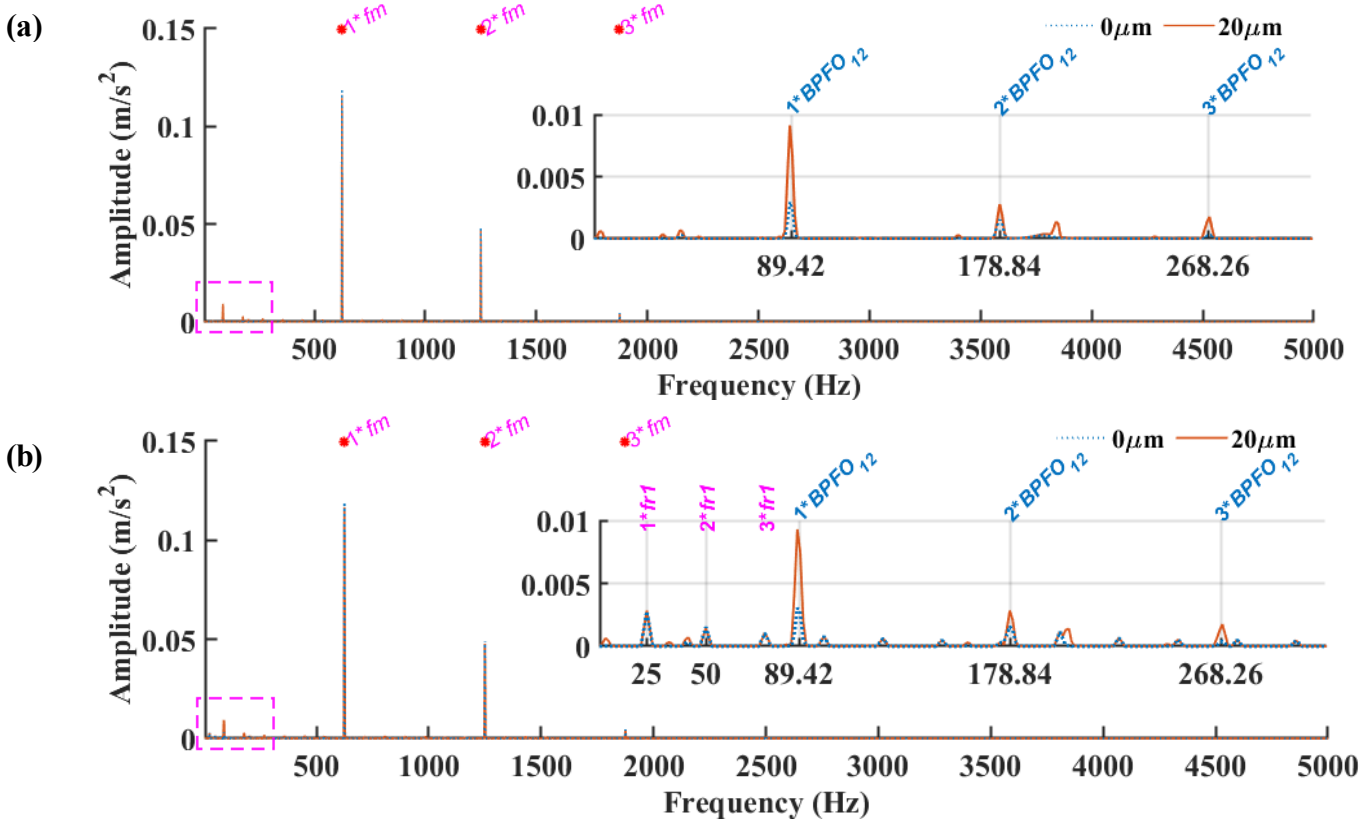

Fig. 5. Envelope spectra on vertical direction of bearing 1,2 under **(a)** bormal gear and **(b)** spalling gear

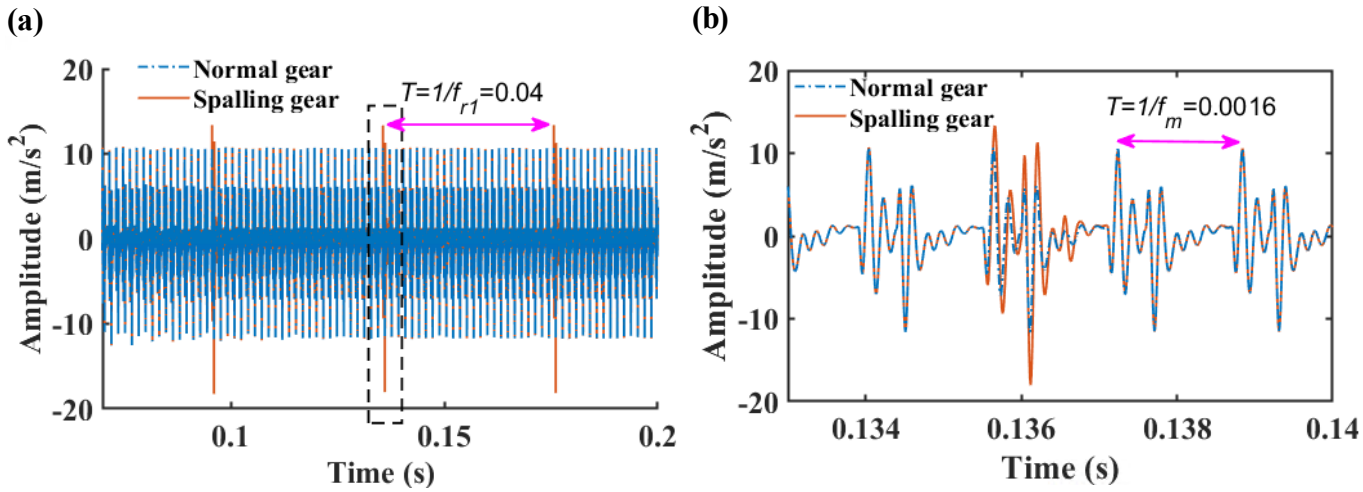

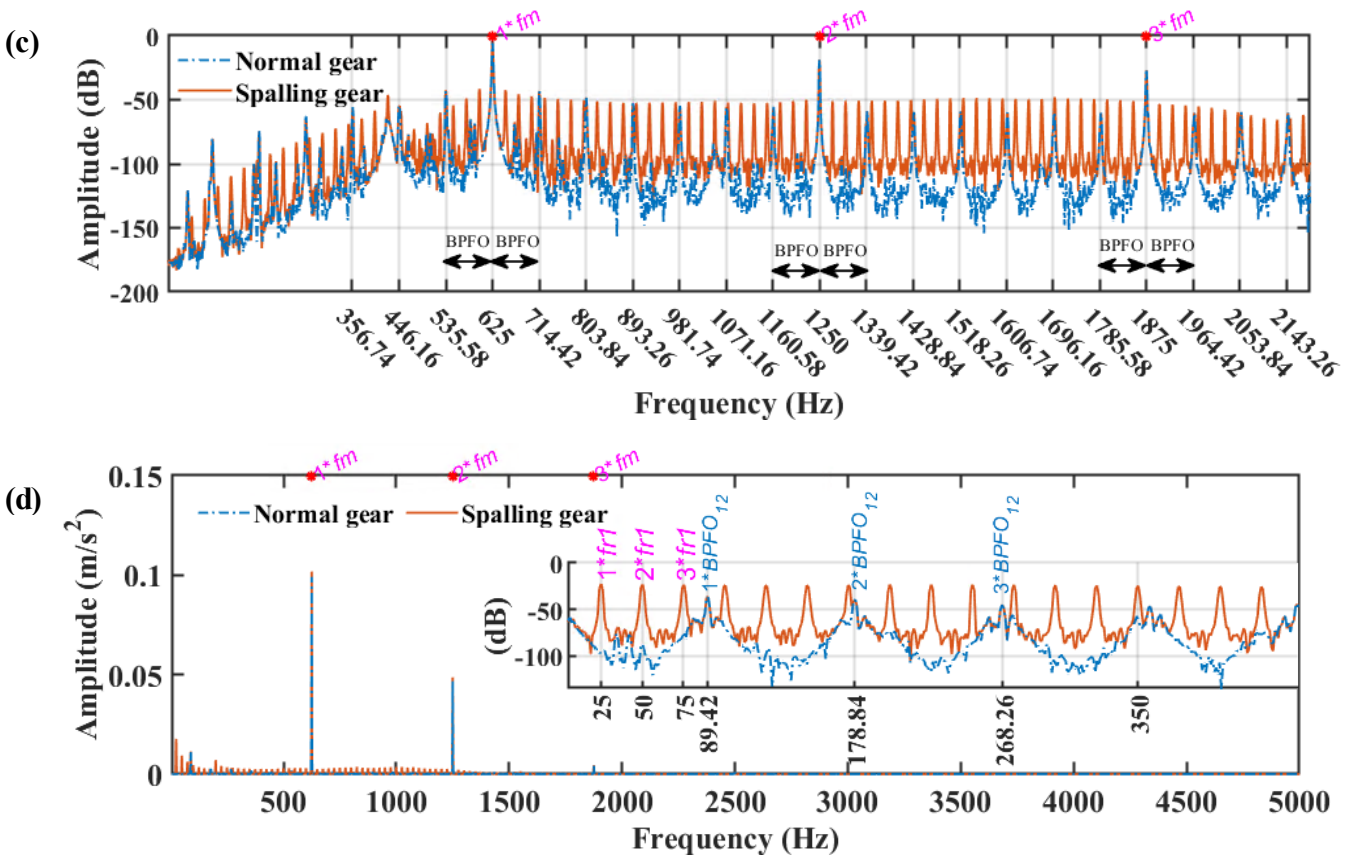

Fig. 6. Numerical simulation results of bearing 1,2 on vertical direction: **(a, b)** waveform **(c)** low frequency band of first three harmonics of GMF and **(d)** envelope spectrum

From **Fig. 6**, it is found that the GMF and its harmonics have higher amplitude due to the gear meshing. In Ref. [20], the authors have found that BPFO is dominant frequency from the envelope spectrum for bearing without obvious local defects and shows an uptrend with the increase of radial clearance. Through aforementioned analysis, for a gear-shaft-bearing system in a gearbox, when there is no fault on gear, BPFO is easy to be distinguished in the spectrum. But when local defect, such as spalling, appears on gears, the amplitude of shaft rotating frequency is more dominant than BPFO, due to the fault gear extracts much more energy in the gearbox. Besides, in a real gearbox with much joint components and background noise, the BPFO is usually weakened by the transmission path and submerged by the other components in the spectrum, which brings much difficulty for bearing health condition monitoring. Even so, in view of the modulation phenomenon between bearing and gear, it should be used for bearing health condition monitoring, instead of seeking for other resonant frequency bands for demodulation. Thus, this study was motivated by this finding.

2.4 Experimental Verification

It is noted that, the model is mainly focus on the system including bearing and gear, and bearing clearance is a factor in the model. Consequently, the verification mainly focuses on the bearing clearances and influence of gear, which consists of two parts. The first part is a strict bearing test rig to verify the influences of bearing clearance on vibration responses, while the second part is a gearbox test rig to verify the vibration responses of the gear-shaft-bearing system.

To show the influence of bearing clearance on vibration, a strict experiment is designed on a bearing test rig, which is shown in **Fig. 7**. Bearing 6205 with clearances of CN and C4 are selected in the experiment duo to that CN is commonly used and there is no overlap between CN and C4. Besides, the rotating speed is 1800rpm, and the sampling frequency is 10240Hz.

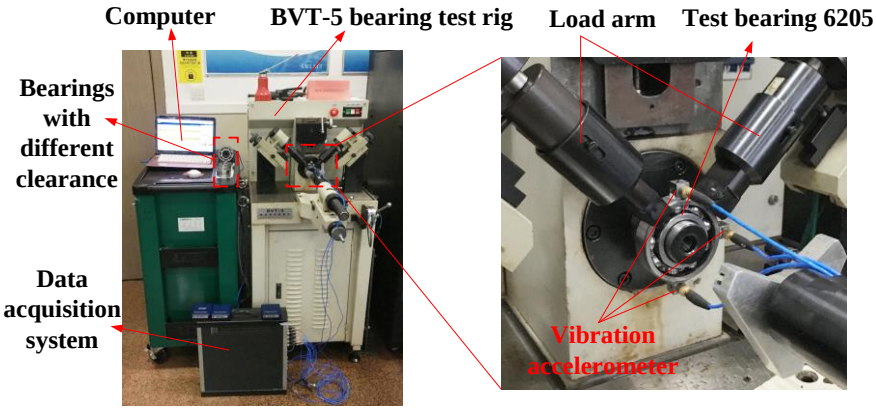

Fig. 7. Bearing test rig

The waveform, FFT spectrum and envelope spectrum are shown in **Fig. 8**. It can be found that C4 is larger than CN form the waveform, and BPFO is distinct in the envelope spectrum. Specially, the amplitude on BPFO of C4 is larger than CN. The result is consistent with the findings in Ref.[20]. However, in Ref.[20], shaft rotating frequency also presents high amplitude in the envelope spectrum. It can be attributed to the structural characteristics of the test rig.

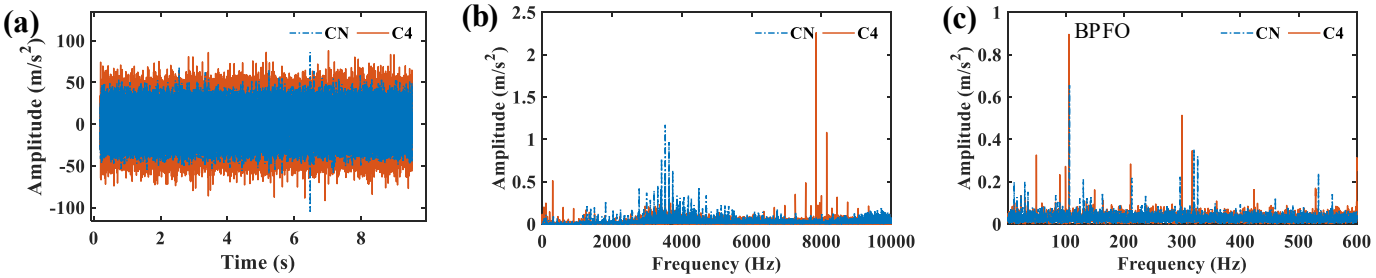

Fig. 8 Bearing test result: **(a)** waveform, **(b)** FFT spectrum and **(c)** envelope spectrum

To verify the effectiveness of the proposed model on modeling the vibration of the system with bearing, shaft and gear, including clearances, normal gear and spalling gear, a two-stage reducer test rig is utilized to measure the vibration signal of rolling element bearing. The experiment setup is as shown in **Fig. 9**. **Table 7** shows the characteristic frequencies under 700, 900 and 1100rpm, including rotational frequency of each shaft, the mesh frequencies and BPFO.

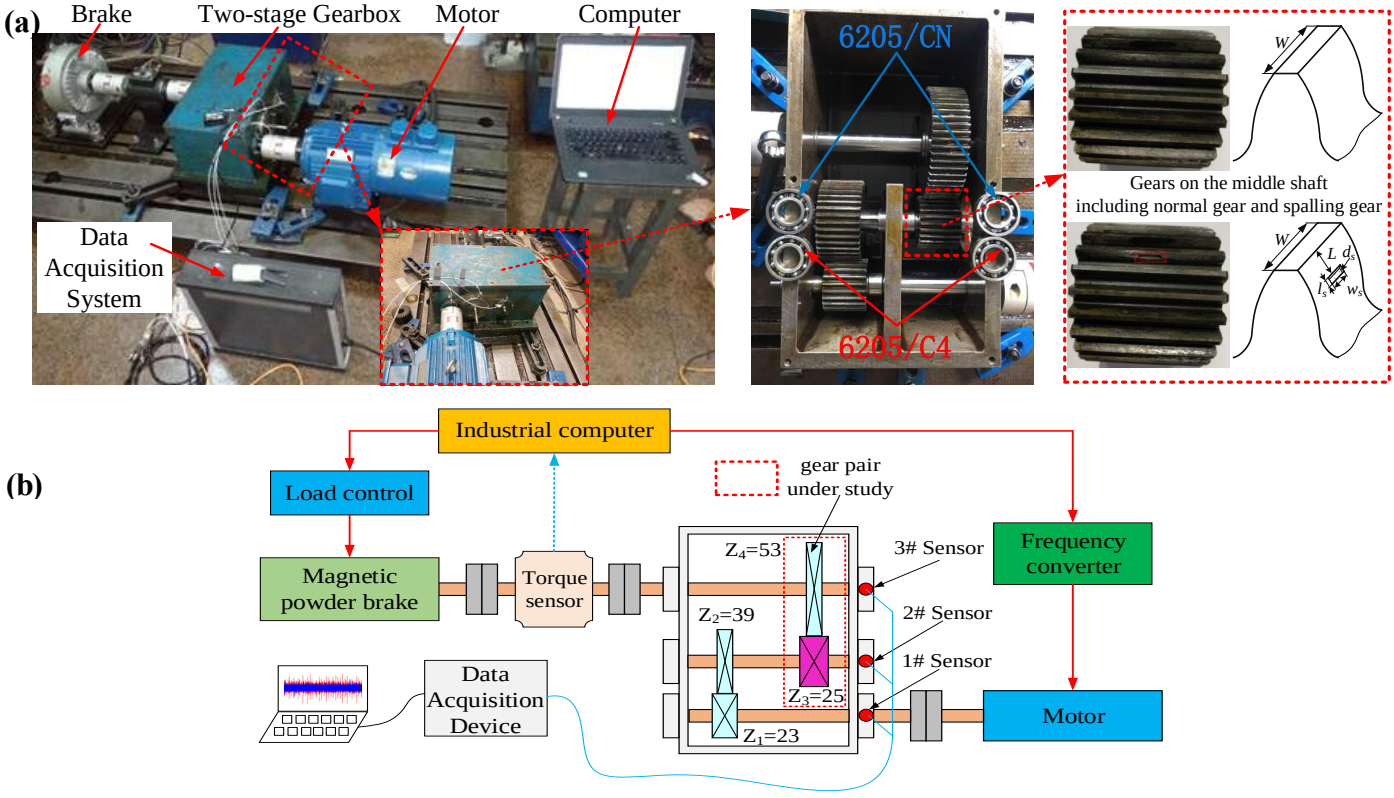

Fig. 9. Experimental setup: **(a)** Gearbox test rig and **(b)** schematic drawing.

Table 7

Characteristic frequencies of Bearing 6205 under different rotational speed

Motor speed	f_{r1}	f_{r2}	f_{r3}	f_{m1}	f_{m2}	BPFO
700	11.67	6.88	3.25	268.33	172.01	24.65
900	15	8.85	4.17	345	221.15	31.69
1100	18.33	10.81	5.10	421.67	270.30	38.74

Note: $f_{m1} = f_{r1}z_1$, $f_{m2} = f_{r2}z_3$

Taking 700rpm as an example, the vibrational responses of bearing on the middle shaft (shaft 2, 412.82 rpm) are shown in **Fig. 10** and **Fig. 11**, including waveform, FFT spectrum and envelope spectrum.

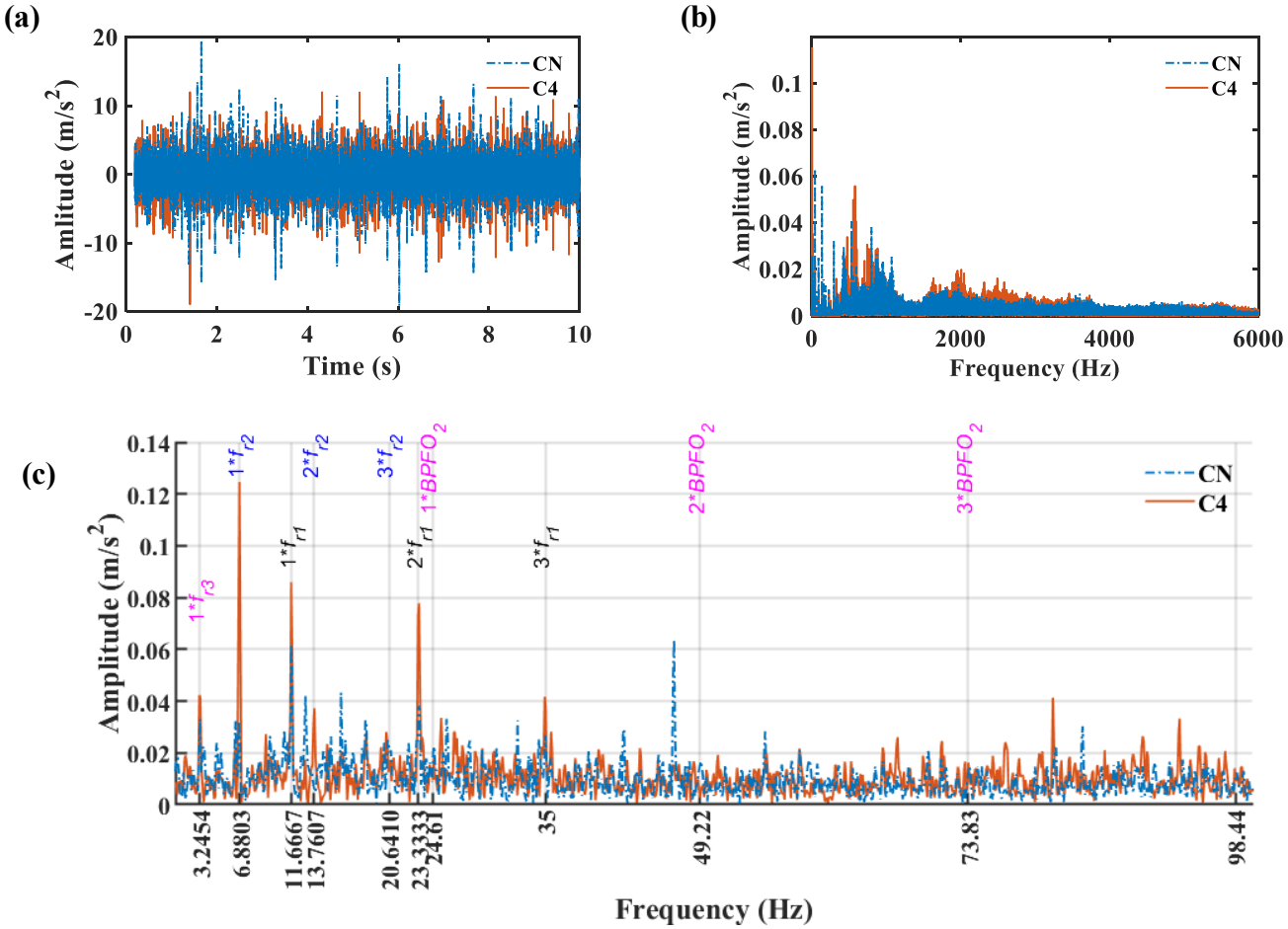

Fig. 10. Normal gear when clearances are CN and C4: **(a)** waveform, **(b)** spectrum and **(c)** envelope spectrum

Form **Fig. 10**, there is no obvious difference between CN and C4, and BPFO is submerged in background noise. However, shaft frequencies, $f_{ri}, i = 1,2,3$ are obvious in the envelope spectrum. The amplitude on shaft frequencies of C4 is larger than CN. It can be attributed to that when bearing clearance becomes larger, the center distance between pinion and gear becomes lager, which is transformed into a kind of 'gear fault'. Under this case, the information of bearings is submerged and hard to discover. From the strict bearing test rig to the gearbox test rig, the information of bearing is weakened gradually when there is no obvious defect on bearings.

Besides, to verify the model on representing vibration system composed of gear, shaft and bearing under the influences of gear meshing, acceleration under normal gear and spalling gear are measured when bearing clearance class is CN. The corresponding analysis is shown in **Fig. 11**.

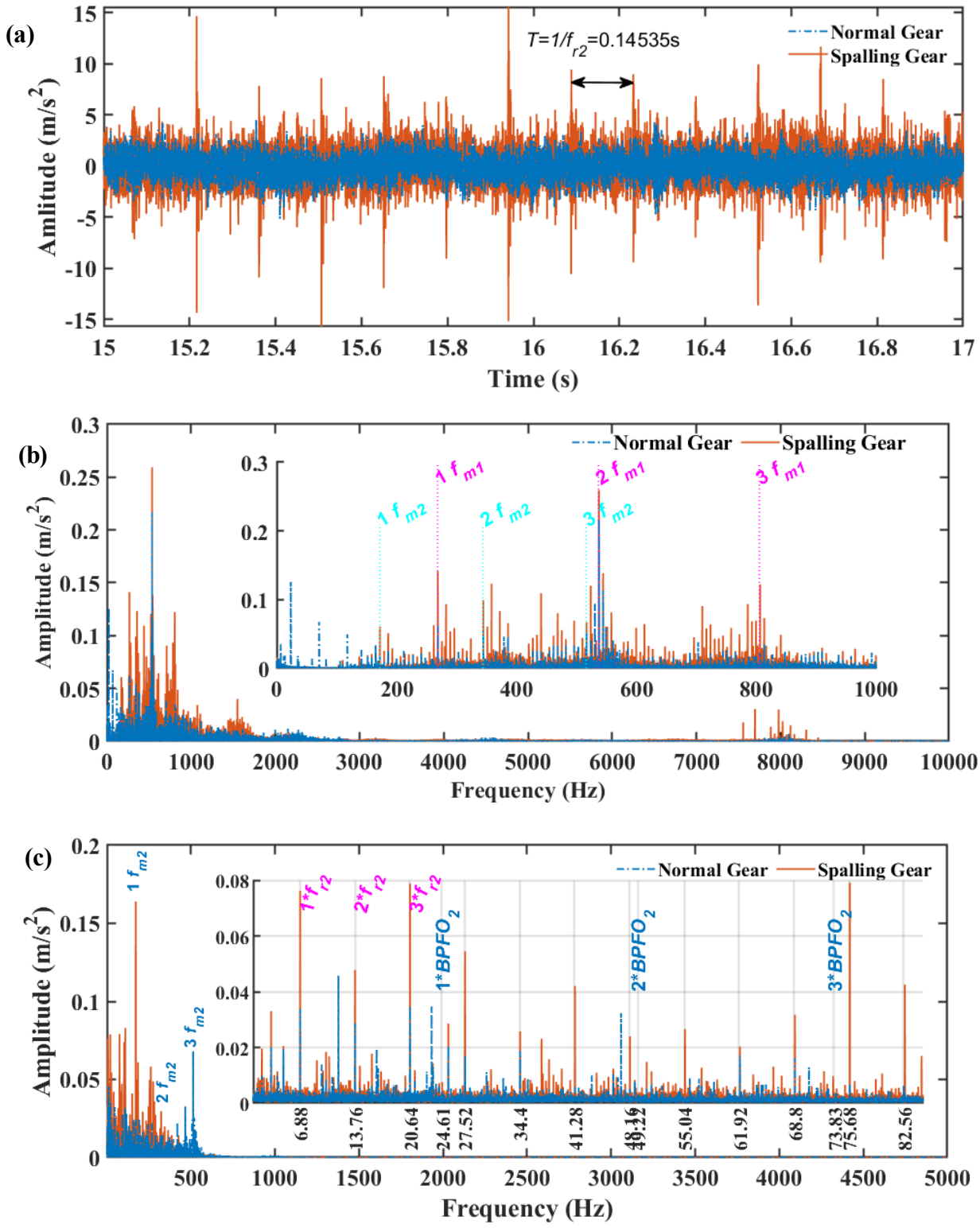

Fig. 11. Comparison between normal gear and gear with spalling: **(a)** time-domain waveform, **(b)** FFT spectrum and **(c)** Envelope spectrum of the test rig data

From **Fig. 11**, it finds that GMF and its harmonics have comparatively higher amplitude. Especially when there is a spalling defect on gear tooth surface, the vibration represents impulsive waveform with the period of $1/f_{r2}$. Through envelope spectrum, which is carried out on the on the narrow frequency band between 0Hz and $3.5 \times f_{m2}$, the rotating frequency of the shaft supporting the faulty gear, i.e., f_{r2}, as well as its harmonics, can be obviously recognized especially when there is a spalling defect on gear, which is consistent with simulation.

Overall, based on above analysis, the model has better performance on modeling the vibration of the gear-shaft-bearing system, including normal gear and spalling gear. However, the bearing characteristic frequency, i.e., BPFO of the middle shaft is not obvious with smaller amplitude. This can be attributed to that the bearing is normal with small clearance, and the

impulse of ball pass is weak. Besides, for the real test, errors from geometry and assembly are inevitable, which contaminated the feature of bearing. On the other hand, seeking for other indicators for bearing weak feature extraction will be a meaningful and challenge work. Even though the BPFO was not distinctive; the results are consistent with the simulation in Section 2.3 from that of time-domain and frequency-domain, which provides evidence for the effectiveness and accuracy of the proposed model.

3 Bearing Characteristics with Different Radial Clearances in a Gearbox

To model the bearing vibrations, efforts can be found through literatures. However, few scholars paid attention to the different classes of bearing clearance, which should be taken into account. On one hand, when selecting bearing before operation, there are five classes clearance in ball bearing, i.e., C2, CN (Normal), C3, C4 and C5. The detailed rated value of each class of clearances after manufacturing is depicted in **Table 8**. On the other hand, bearing clearances will increase due to the various wear during the lifetime, which was neglected in most bearing studies. Thus, to complete the understanding of bearing clearances, the clearances are extended from 0 to 90μm with the interval as 10μm. The large clearance represents wear induced scenarios. Note that the rotational speed and the torque load was set as 1500rpm and 60Nm, respectively.

Table 8

Clearance values of deep groove ball bearings[20]

Bore Diameter d (mm)		C2 (μm)		CN (μm)		C3 (μm)		C4 (μm)		C5 (μm)	
over	include	min	max	min	max	min	max	min	max	min	max
---	2.5	0	6	4	11	10	20	---	---	---	---
2.5	6	0	7	2	13	8	23	---	---	---	---
6	10	0	7	2	13	8	23	14	29	20	37
10	18	0	9	3	18	11	25	18	33	25	45
18	24	0	10	5	20	13	28	20	36	28	48
24	30	1	11	5	20	13	28	23	41	30	53
30	40	1	11	6	20	15	33	28	46	40	64
40	50	1	11	6	23	18	36	30	51	45	73
50	65	1	15	8	28	23	43	38	61	55	90

3.1 Effect of Gear Dynamics on Bearing Clearances

For normal gear and spalling gear, the time varying mesh stiffness (TVMS) and dynamic mesh force, can be calculated according to Eq. (29) and Eq. (30). From **Fig. 12 (a)** and **(b)**, it can be seen that the mesh force exhibits an impulse with the varying of TVMS. Especially, TVMS decreases with the increase of spalling size, while the dynamic mesh force increase with the increase of spalling size.

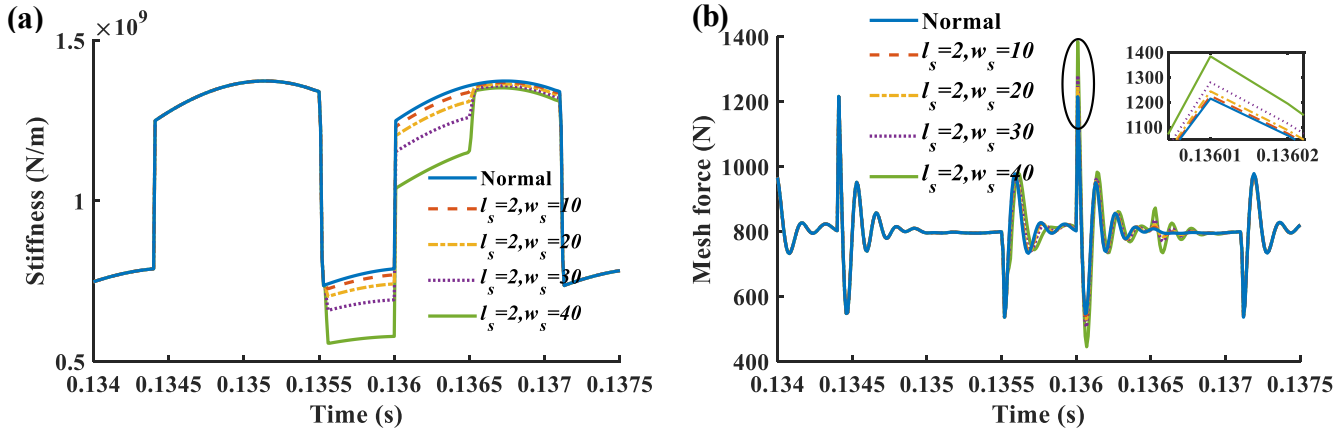

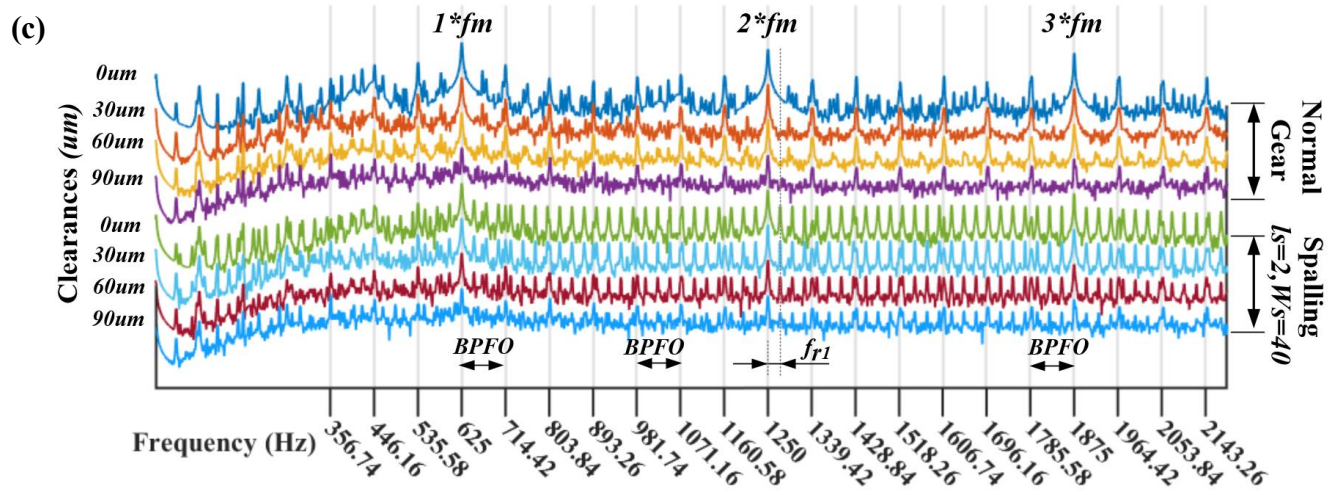

Fig. 12. Numerical results: **(a)** TVMS, **(b)** dynamic mesh force, **(c) FFT** spectrum of first three GMF harmonics

Corresponding to the changes in forces, bearing vibration in vertical direction is presented in the frequency domain as shown in **Fig. 12 (c)**. As can be seen, GMF and its harmonics are dominant through the FFT spectrum. Sideband of BPFO can be found around the GMF and its harmonics. To reveal the modulation in detail, envelope spectrum is shown in **Fig. 13(a)**, which shows that the modulation becomes more obvious with the increase of bearing clearances, resulting in higher amplitudes on BPFO. **Fig. 13(b)** depicts amplitude at shaft rotating frequency f_{r1} and BPFO extracted from the envelope spectrum. When gear is normal or gear spalling size is relatively small, usually at an earlier operation time, the amplitude of BPFO is higher than gear fault frequency f_{r1} and the BPFO increases with the clearances. During this period, the diagnostic feature of bearing is obvious. However, when spalling size increases during the operations, e.g., caused by mild wear, the amplitudes at gear fault frequency f_{r1} increase with the spalling size and become higher than BPFO. It means that the influence of gear fault start induce stronger impact on the system, which will submerge bearing signals and bring difficulty for bearing detection. It should be noted that the above analysis does not consider the influences of background noise and transmission path in the vibration system. Under the comprehensive effect of gear defects, noise and energy dissipation, BPFO amplitude will be more invisible and difficult for bearing clearances feature extraction and monitoring. Efficient signal processing tools must be used to suppress these influences in order to accurately diagnose changes in bearing clearances.

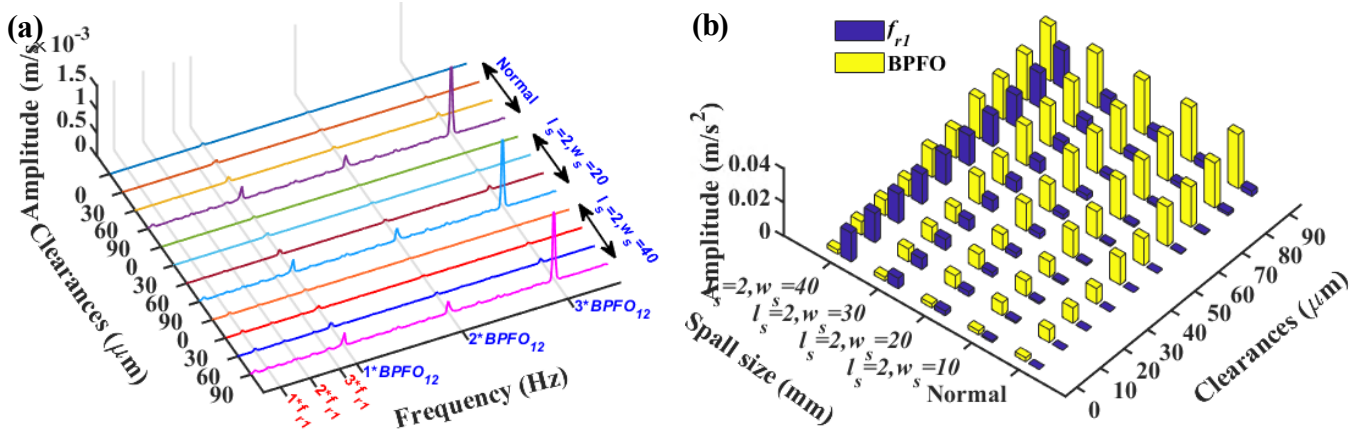

Fig. 13. Envelope spectrum of **(a)** normal gear and two spalling gear cases and **(b)** characteristic frequencies amplitudes

3.2 Bearing Clearance Indicators Based on MSB-SE

Modulation Signal Bispectrum (MSB) [34][35][36] has been proved to be an effective method in denoising and sparse representation, as well as demodulating multiple frequency components in noisy signals for bearing and motor condition monitoring. Particularly, for gearbox monitoring, MSB has shown great effectiveness when cleaning envelope signals based on vibration data. Consequently, MSB is utilized in this study to capture weak clearance signatures in vibration data from a gearbox system. MSB is derived from conventional bispectrum (CB) which is expressed in frequency domain as

$$B(f_c, f_x) = E < \mathrm{X}(f_c)\mathrm{X}(f_x)X^*(f_c + f_x) > \quad (27)$$

where X(f) is the discrete Fourier transform (DFT) of the time-domain signal $x(t)$, X*denotes the complex conjugate of X(f), E <> stands the expectation operator, f_c, f_x and $f_c + f_x$ are from three different frequency components. CB possesses better performance on suppressing random noise and shows a peak at different nonlinear interacted components in the bispectrum after calculation by Eq.(7). Based on CB, MSB takes into account the possibility of frequency component $f_c - f_x$, whose existence may be also resulted from the nonlinear interaction between f_c and f_x in the modulated signal. Therefore, MSB is given as

$$B_{MS}(f_x, f_c) = E[X(f_c + f_x)X(f_c - f_x)X^*(f_c)X^*(f_c)] \tag{28}$$

where f_x denotes the faulty or modulation frequency; f_c denotes the carrier frequency. If there was a interaction between the f_x and f_c, a bispectral peak will appear at the bifrequency (f_c, f_x). Besides, MSB considers the amplitudes of $f_c + f_x$ and $f_c - f_x$ all together to make the sideband characteristics more precise and obvious even for modulation signals with high intensity noise.

After MSB calculation, the magnitudes under different clearance are shown in **Fig. 14**. It is noted that for the spalling gear, the spalling size was set of $l_s = 2mm$ and $w_s = 20mm$, while the depth of the spalling d_s and the distance between the spalling and the pinion top was set as 1mm and 1.8mm, respectively.

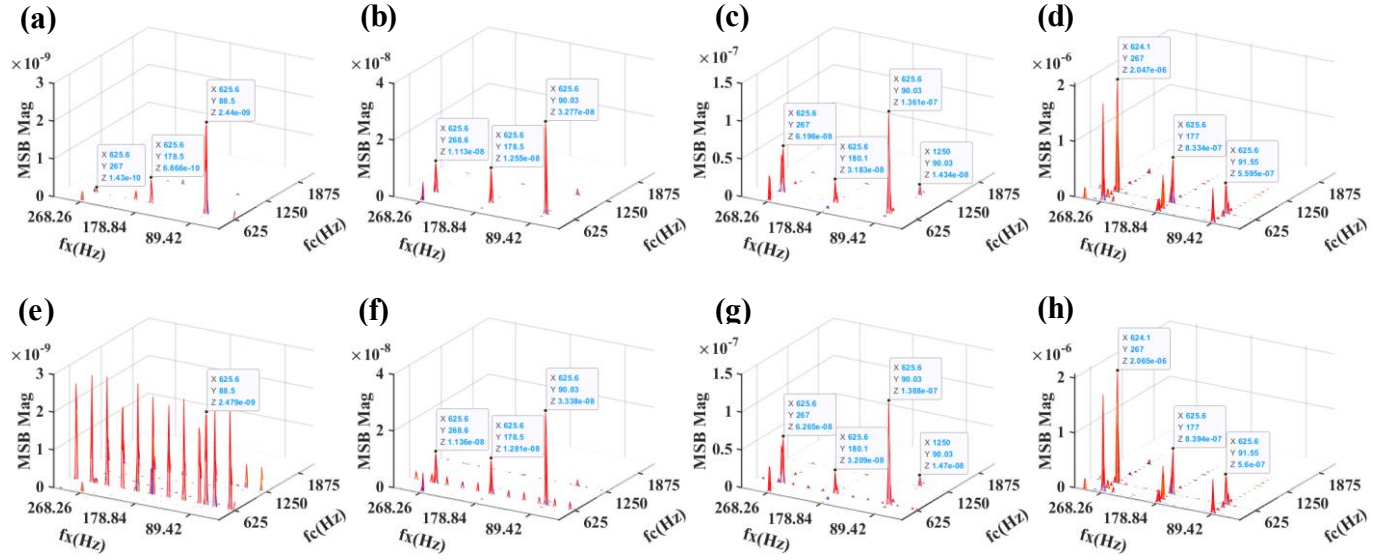

Fig. 14. MSB Magnitude of **(a)** normal gear-0μm, **(b)** normal gear-30μm, **(c)** normal gear-60μm, **(d)** normal gear-90μm, **(e)**spalling gear-0μm, **(f)** spalling gear-30μm, **(g)**spalling gear-60μm and **(h)**spalling gear-90μm

The MSB results show better performance for bearing clearances signature extraction. However, when calculating the expectation of the f_c, f_x, $f_c - f_x$ and $f_c + f_x$ in MSB, both the effect of f_c and f_x are included in the $B_{MS}(f_x, f_c)$. It means that both the influence of GMF and bearing BPFO are mixed together in the result. Under this case, it cannot distinguish which one, i.e., gear mesh or bearing clearance, result in the change of B_{MS}. Thus, getting rid of the influence of carrier frequency, i.e., GMF, will be benefit to the bearing clearance monitoring.

To address this problem, MSB-SE was proposed based on original MSB. The MSB-SE [34] can be defined in the frequency domain as,

$$B_{MS}^{SE}(f_x, f_c) = E[X(f_c + f_x)X(f_c - f_x)X^*(f_c)X^*(f_c)/|X(f_m)|^2] \tag{29}$$

It means that the modulation frequency f_c was normalized and sideband can be quantified without the effect of carrier frequency. Under this circumstance, the effect of sideband, i.e., bearing clearance, can be monitored through MSB-SE without the influence of GMF amplitude. Inspired by this, MSB-SE has better capacity to monitor the change of bearing clearances in a gearbox. In this study, considering the complexity of modulation, both three harmonics of BPFO and f_m were included to generate the indicator for monitoring bearing clearance. The sum of the potential nine MSB-SE magnitudes, i.e., (1,2,3) ×BPFO modulated on (1,2,3) × f_m, are calculated, which are shown in **Fig. 15**.

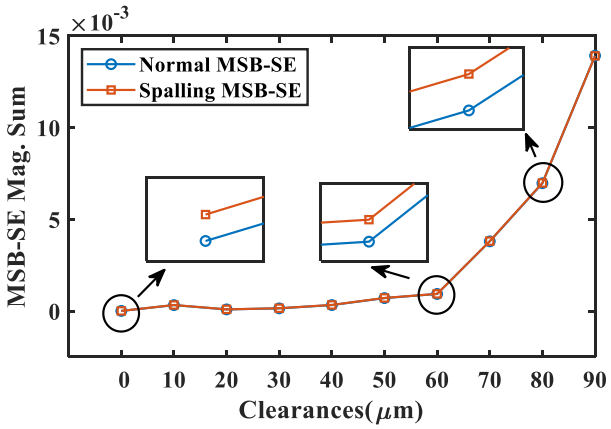

Fig. 15. MSB-SE magnitudes under different clearances

When using MSB-SE to extract signatures of bearing clearance, the indicator shows an uptrend with the increase of clearances under both normal and spalling gear. Besides, slight difference can be found between normal gear and spalling gear after normalizing the GMF after enlargement, which shows a slight rising on the amplitude of BPFO when gear spalling appears. It could be attributed to that even the influence of gear on bearing was deleted through MSB-SE, according to the coupling between them in the vibration model, the gear spalling will influence the motion of bearing and accelerate the wear of bearing, leading to larger clearance.

4 Experiment Verification on MSB-SE indicator

4.1 Evaluation with Gearbox Run-to-Failure Datasets

To evaluate the performance developed, datasets from a gearbox run-to-failure test is adopted to estimate the health conditions of the 6 bearings in the tested gearbox, which was carried out in the Condition Monitoring Laboratory at University of Huddersfield and aims to study the progressive deteriorations of gearbox when mimicking real working conditions. The test has operated for 838 hours without any interactions until it was found there is an apparent growth in vibrations of the gearbox at GMFs. After long-time operation, the offline inspections show that wear, caused by the increased gear meshing, appeared the gear tooth surfaces [36], as shown in **Fig. 17**. However, bearing health conditions are ignored at first due to there are no obvious characteristic vibrations during the long-time operation, even though there are some light wear markers on the bearing raceways after offline inspections. Thus, in this study, the datasets are analyzed focusing on bearing clearances.

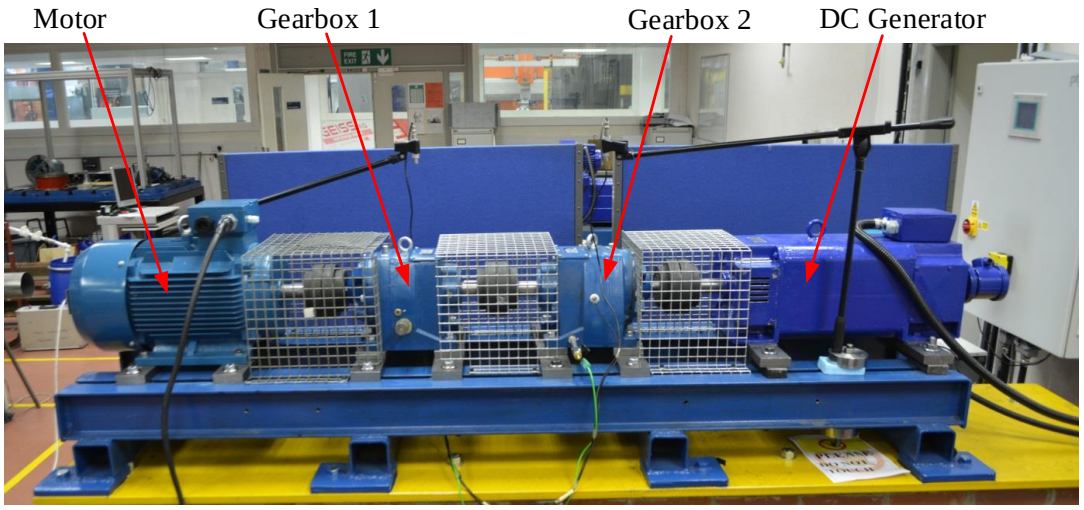

Fig. 16. Run-to-failure gearbox test rig

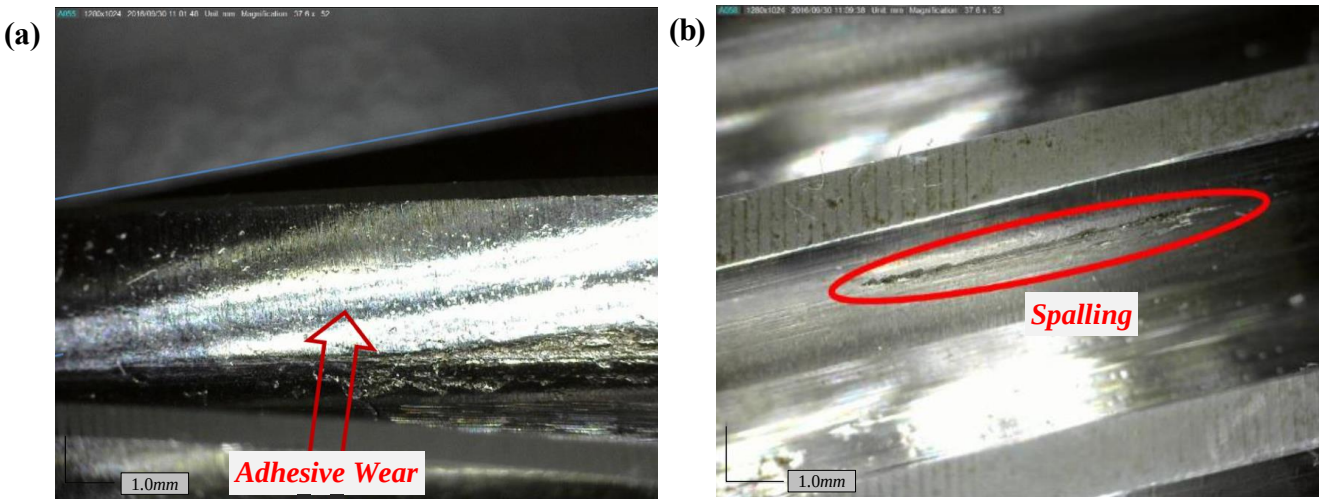

Fig. 17. Gear and bearing offline inspections: (a) gear wear and (b) gear spalling

To facilitate the analysis, **Fig. 18** also gives the details of bearing arrangements. In each gearbox, there are two pairs of helical gear and three shafts supported by six bearings detailed in **Fig. 18**. **Table 9** and **Table 10** also presents the relevant frequency values of gears and bearings at the operating speed of 1036.8rpm, respectively. In addition, for cost effective condition monitoring implementation, one accelerometer was attached on the gearbox housing close to bearings B3 and B5. Under this case, the acquired vibration data shows lower SNR, which provides more challenge for the bearing signatures extraction and the proposed indicator.

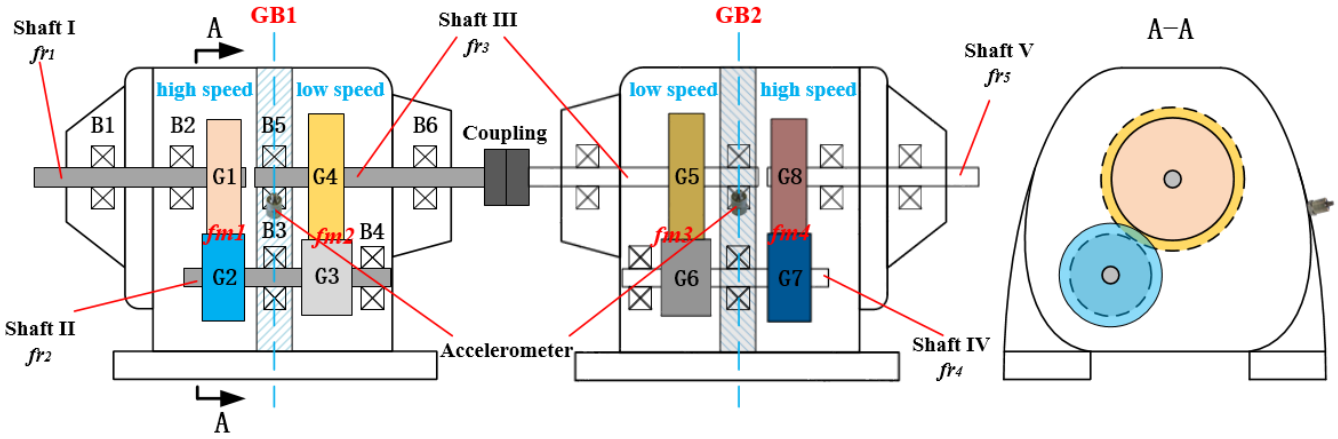

Fig. 18. Schematic diagram of the two-stage helical gearbox

Table 9

Gearbox parameters and characteristic frequencies

Gearbox parameters		Value
Tooth number	Z_{G1}/Z_{G2}, Z_{G3}/Z_{G4}	49/55, 13/59
	Z_{G5}/Z_{G6}, Z_{G7}/Z_{G8}	59/13, 47/58
Shaft frequency	$f_{r1} = speed/60$	17.28
	$f_{r2} = f_{r1}Z_{G1}/Z_{G2}$	15.39
	$f_{r3} = f_{r2}Z_{G3}/Z_{G4}$	3.39
	$f_{r4} = f_{r3}Z_{G5}/Z_{G6}$	15.39
	$f_{r5} = f_{r4}Z_{G7}/Z_{G8}$	12.48
Mesh frequency	$f_{m1} = f_{r1}Z_{G1}$	846.72
	$f_{m2} = f_{r2}Z_{G3}$	200.07
	$f_{m3} = f_{r3}Z_{G5}$	200.07
	$f_{m4} = f_{r4}Z_{G7}$	723.33

Table 10

Bearing specification and nominal characteristic frequency

Bearing name	B1	B2	B3 & B4	B5	B6
Bearing type	6206	6207	6305	6207	6308
Clearance level	C3	C3	C3	C3	C3
Shaft Frequency (Hz)	f_{r1}=17.28	f_{r1}=17.28	f_{r2}=15.39	f_{r3}=3.39	f_{r3}=3.39
BPFO (Hz)	61.6	61.6	39.6	12.0	10.4

To give a qualitative indication of the bearing health conditions, this proposed method is used for diagnosing the change in radial clearances based on a number of data sets at representative time instances. These datasets are chosen from 838 data records collected hourly during the course of the test, being easier for result presentation in verifying the performance. **Fig. 19** depicts the waveforms and some commonly used statistical indicators from time domain. From the figure, during 838 hours operation, the vibration shows seldom increase but with fluctuations. **Fig. 20** shows the envelope spectra under different operating time. As can be seen, the bearing clearance characteristic frequencies (BPFOs) were submerged into the spectra. Especially, taking bearing3,4 and bearing 5 as an example, BPFO and its harmonics show different trend, as shown in **Fig. 21**, which is difficult for indicating the change of bearing clearances.

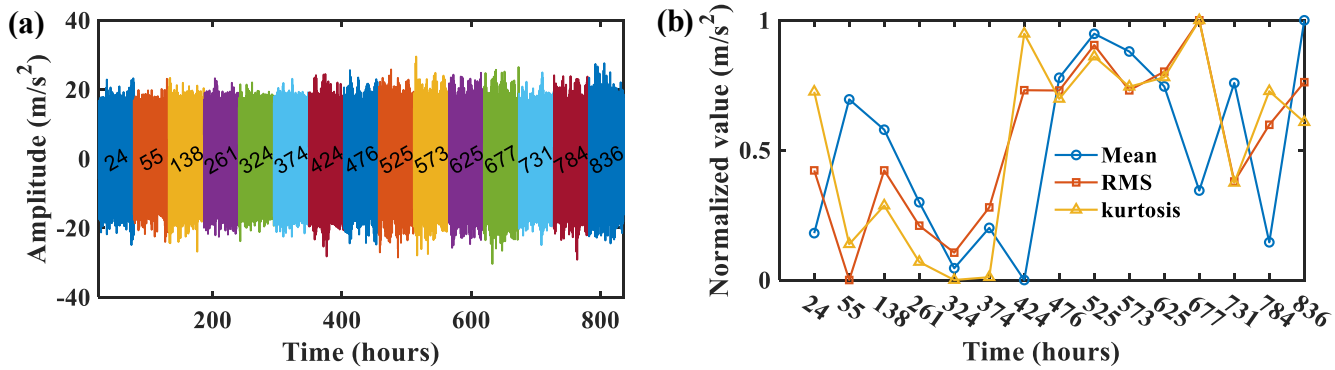

Fig. 19. Time-domain at 15 of successive time instants: **(a)** waveforms and **(b)** indicators

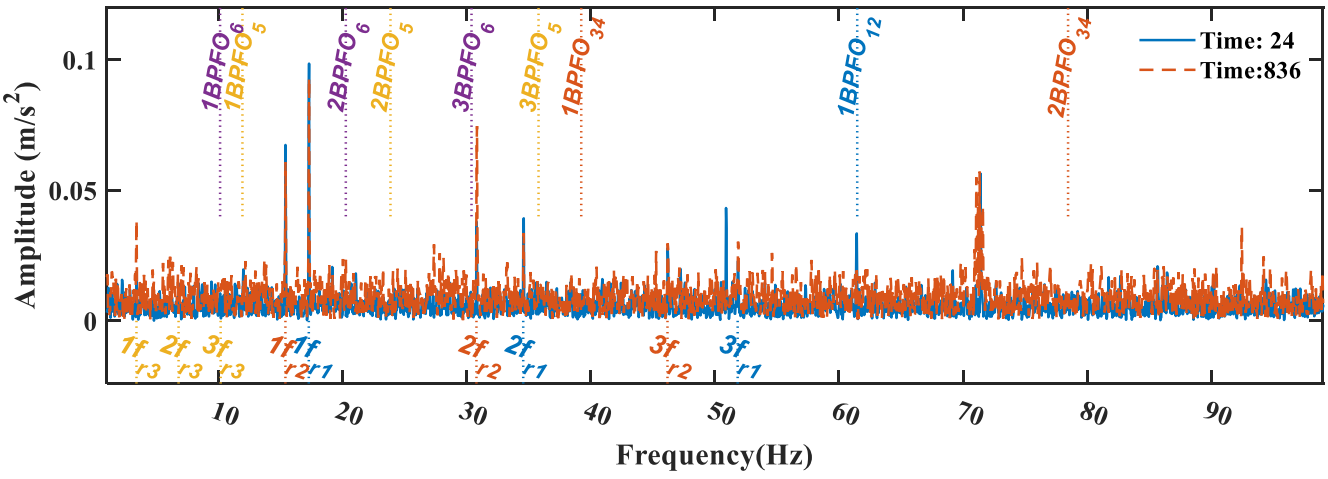

Fig. 20. Envelope spectrum under different operating time

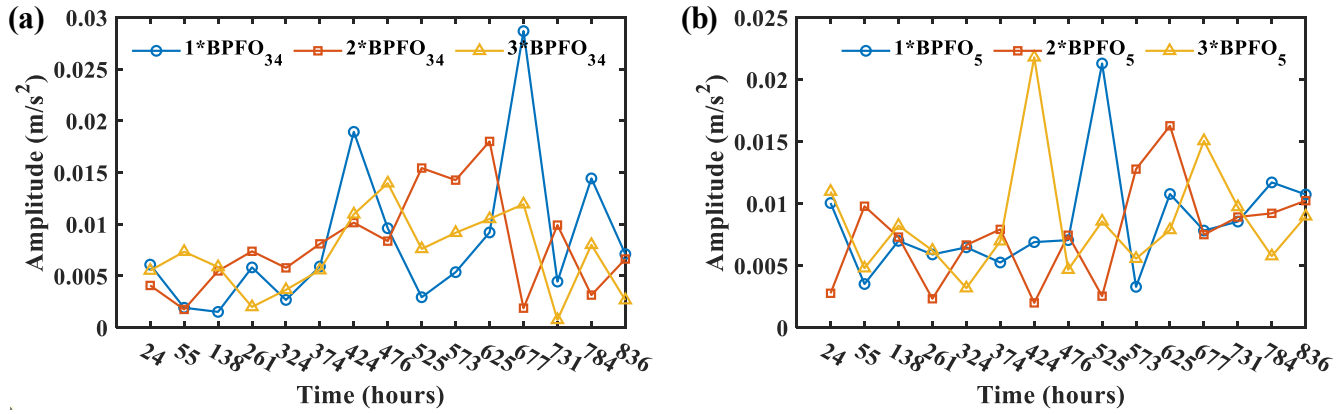

Fig. 21. BPFO amplitudes of different bearing: **(a)** B3,4 and **(b)** B5

4.2 Clearance Diagnostics of Different Bearings

Taking bearing 3,4 as an example, the MSB-SE magnitudes at operating time of 24 are shown in **Fig. 22**. It is noted that the show MSB-SE magnitude are selected from different harmonics of BPFO and f_m.

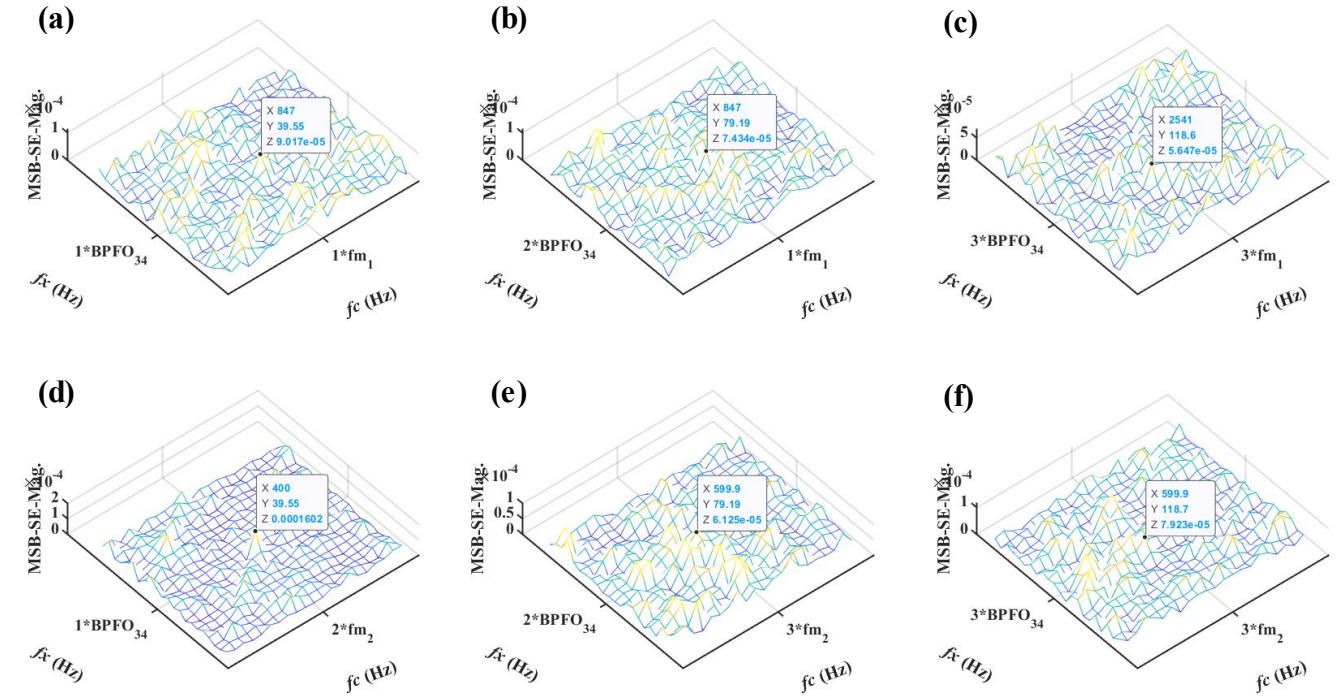

Fig. 22. MSB-SE Magnitude at operating time of 24

In the similar way, considering the complexity of modulation, the amplitude of three harmonics of BPFO and f_m, i.e., (1,2,3) ×BPFO modulated on (1,2,3) × f_m, were added together to generate the indicator for monitoring bearing clearance. The MSB-SE results of six bearings in gearbox 1 are shown in **Fig. 23**. It is noted that the indicator vary not too much, which could be attributed to that the clearances increase within a comparatively smaller range. After the run-to-failure experiment, during the process of offline inspection, the bearing clearance was measured, which increased about 20μm.

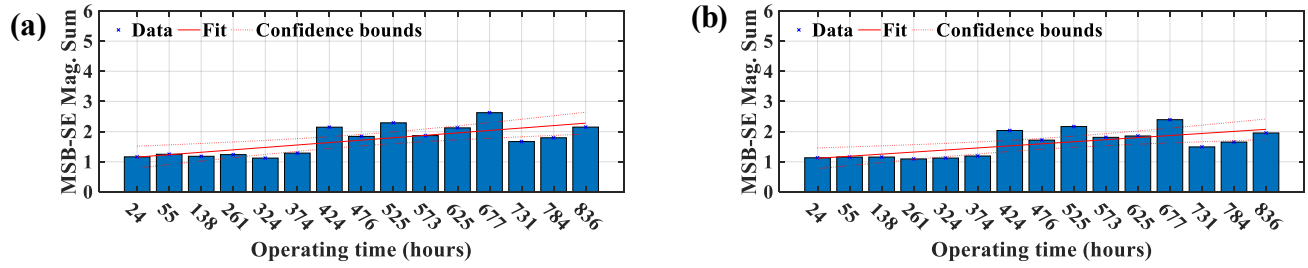

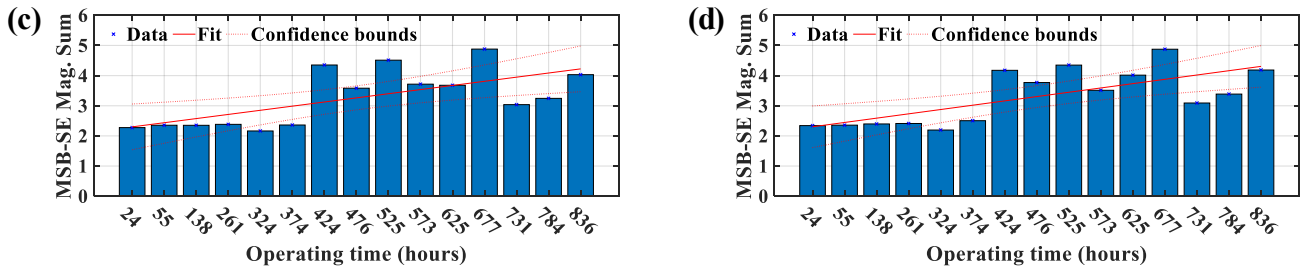

Fig. 23. Bearing clearances monitoring based on MSB-SE magnitude: **(a)** B1,2, **(b)** B3,4, **(c)** B5 and **(d)** B6

As can be seen **Fig. 23**, the six bearings show uptrends with certain fluctuations during the operation. The fluctuation can be attributed to the environment and noise effect. It should be noted that the bearing 1 and bearing 2 have the same characteristic frequency (BPFO). Thus, the MSB-SE contains the clearances change of these two bearings. Duo to the limit of the number of sensors, it is difficult to distinguish them. Here, it is assumed that bearing 1 and bearing 2 have the same clearances variance and shared the calculated the total indicator value. It has adopted same operation to deal with bearing 3 and bearing 4.

To comparison the performance of MSB-SE and BPFO, monotonicity [43][44] are adopted to verify the performance of the indicators. As expounded in literature, monotonicity can discover whether there is a trend about the indicator and higher monotonicity shows a better upward (or downward trend). The higher comprehensive value, the better performance. The result is shown in **Table 11** and **Fig. 24**.

.

$$monotonicity(x) = \frac{1}{K-1}\left|\sum_k \delta\left(X_T(t_{k+1}) - X_T(t_k)\right) - \sum_k \delta\left(X_T(t_k) - X_T(t_{k+1})\right)\right| \quad (30)$$

where $X(t_k)$ is the degradation feature value at time t_k, $X_T(t_{k+1})$ is its trend value, K is the total number of observing times and function $\delta(\cdot)$is the simple unit step function.

Table 11

Monotonicity value of BPFO and MSB-SE

Bearing	Indicator	Monotonicity value
B12	BPFO	0.1429
	MSB-SE	0.5714
B34	BPFO	0.4286
	MSB-SE	0.5571
B5	BPFO	0.2857
	MSB-SE	0.4286
B6	BPFO	0.1428
	MSB-SE	0.5714

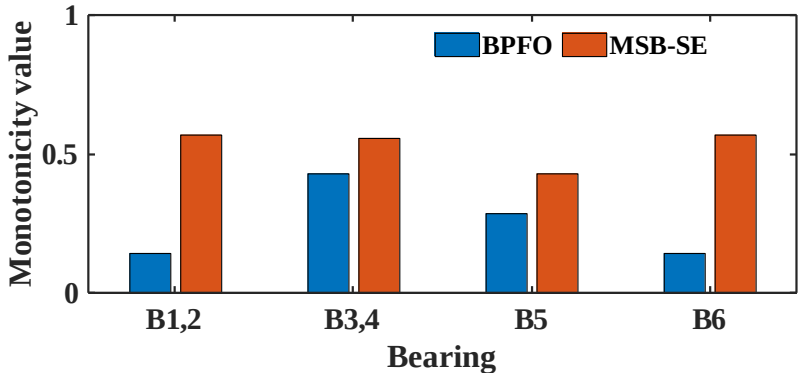

Fig. 24. Monotonicity value of BPFO and MSB-SE

Overall, the proposed MSB-SE indicator shows better performance on monitoring bearing clearances over BPFO, and

some other statistical indicators, such as mean value, RMS and kurtosis.

5. Conclusions

Aiming at evaluating the bearing health conditions at initial operations, a gear-shaft-bearing-housing dynamic model has been proposed to investigate the vibration responses of bearing radial clearances under the effect of gear meshing and a run-to-failure gearbox test rig was designed to validate the effectiveness of the proposed indicator based on MSB-SE for bearing clearances monitoring. Some conclusions which are helpful for bearing clearance monitoring are listed below.

1. The verified gear-shaft-bearing-housing dynamic model is reasonable to describe the interaction and modulation between bearings and gears. When the gear in the gear-shaft-bearing-housing system is healthy, the BPFO is the dominating exciting sources through the envelope spectrum and increases with bearing clearances. When spalling appears on gear surfaces, the gear fault characteristic frequency increases with the spalling size and exceeds BPFO amplitude at a larger spalling size.
2. MSB-SE analysis based on the envelope of the time-domain signal is competent as an efficient tool of purifying the interferences of gear meshing and strong noises, exhibiting better capacity to accurately extract small signatures for indicating bearing clearances variance online. The indicative result shows consistency with the irreversible bearing wear.
3. Through a noisy run-to-failure gearbox test rig, the indicator for each bearing in gearbox shows better performances for bearing clearances monitoring when comparing with RMS, kurtosis and BPFO amplitude from traditional envelope spectrum.

Acknowledgments

This work was supported by Key Program of National Natural Science Foundation of China (52035002), National Natural Science Foundation of China (Grant No. 51905053).

References

[1] Z. Chen, Y. Shao, Dynamic simulation of spur gear with tooth root crack propagating along tooth width and crack depth, Eng. Fail. Anal. 18 (8) (2011) 2149–2164.
[2] L. Jing, M. Zhao, P. Li, A convolutional neural network based feature learning and fault diagnosis method for the condition monitoring of gearbox, Measurement 111 (2017) 1–10.
[3] L. Wang, Y. Shao, Fault mode analysis and detection for gear tooth crack during its propagating process based on dynamic simulation method, Eng. Fail. Anal. 71 (2017) 166–178.
[4] L. Wang, Y. Shao, Fault feature extraction of rotating machinery using a reweighted complete ensemble empirical mode decomposition with adaptive noise and demodulation analysis, Mech. Syst. Sig. Process. 138 (2020) 106545
[5] D. Zhen; J. Guo; Y. Xu; A Novel fault detection method for rolling bearings based on non-stationary vibration signature analysis, Sensors 19 (2019) 3994.
[6] Y. Wang; G. Xu; Q. Zhang; Rotating speed isolation and its application to rolling element bearing fault diagnosis under large speed variation conditions, J. Sound Vib. 348 (2015) 381–396.
[7] H.D.M. De Azevedo; A.M. Araújo; N. Bouchonneau, A review of wind turbine bearing condition monitoring: State of the art and challenges, Renew. Sustain. Energy Rev. 56 (2016) 368–379.
[8] N. Tazi; E. Châtelet, Y. Bouzidi, Wear analysis of wind turbine bearings, Int. J. Renew. Energy Res. 7 (2017) 2120–2129.
[9] A. Chudzik, B. Warda, Effect of radial internal clearance on the fatigue life of the radial cylindrical roller bearing, Eksploat Niezawodn, 21 (2019) 211–219.
[10] F.B. Oswald, E.V. Zaretsky, J.V. Poplawski, Effect of internal clearance on load distribution and life of radially loaded ball and roller bearings, Tribol. Trans. 55 (2012) 245–265.
[11] R. D'Amato, R. Calvo, A. Ruggiero, Measurement capabilities for ball bearing wear assessment, Proced. Manuf. 13 (2017) 647–654.
[12] J. Halme, P. Andersson, Rolling contact fatigue and wear fundamentals for rolling bearing diagnostics -state of the art, Proceed. Inst. Mech. Eng., Part J: J. Eng.Trib. 224 (2009) 377–393.
[13] I. Rehab, X. Tian, F. Gu, The influence of rolling bearing clearances on diagnostic signatures based on a numerical simulation and experimental evaluation, Int. J. Hydromechatronics, 1 (1) (2018) 16–46.
[14] T.A. Harris, Rolling bearing analysis, John Wiley, New York, 2001.
[15] M. Yakout, M.G.A. Nassef, S. Backar, Effect of clearances in rolling element bearings on their dynamic performance, quality and operating life, J. Mech. Science Tech. 33(5) (2019) 2037–2042.
[16] C. Bai, Q. Xu, Dynamic model of ball bearings with internal clearance and waviness, J. Sound Vib. 294 (2006) 23–48.
[17] S.P. Harsha, Rolling bearing vibrations-the effects of surface waviness and radial internal clearance, Int. J. Comput. Meth. Eng. Science Mech. 7 (2) (2006) 91–111.
[18] S.H. Upadhyay, S.P. Harsha, S.C. Jain, Analysis of nonlinear phenomena in high speed ball bearings due to radial clearance and unbalanced rotor effects, J. Vib. Control 16 (1) (2010) 65–88.

[19] Y. Zhuo, X. Zhou, C. ang, Dynamic analysis of double-row self-aligning ball bearings due to applied loads, internal clearance, surface waviness and number of balls, J. Sound Vib.333 (23) (2014) 6170–6189.
[20] M. Xu, G. Feng, Q. He, Vibration characteristics of rolling element bearings with different radial clearances for condition monitoring of wind turbine, Appl. Sci. 10 (2020) 4731.
[21] N. Sawalhi, R.B. Randall, Simulating gear and bearing interactions in the presence of faults –Part I: The combined gear bearing dynamic model and the simulation of localised bearing faults, Mech. Syst. Sig. Process. 22 (2008) 1924–1951.
[22] N. Sawalhi, R.B. Randall, Simulating gear and bearing interactions in the presence of faults –Part II: Simulation of the vibrations produced by extended bearing faults, Mech. Syst. Sig. Process. 22 (2008) 1952–1966.
[23] W. Zeng, X. Zhu, Z. Wei, Study on nonlinear dynamic response of the gear-shaft-housing coupling system, Appl. Mech. Materials, 26-28 (2010) 805–808.
[24] Z. Hu, J. Tang, J. Zhong, Effects of tooth profile modification on dynamic responses of a high speed gear-rotor-bearing system, Mech.Syst. Sig. Process. 76-77 (2016) 294–318.
[25] H. Xiao, X. Zhou, J. Liu, Vibration transmission and energy dissipation through the gear-shaft-bearing-housing system subjected to impulse force on gear, Measurement, 102 (2017) 64–79.
[26] A. Fernandez-Del-Rincon, P. Garcia, A. Diez-Ibarbia, Enhanced model of gear transmission dynamics for condition monitoring applications: effects of torque, friction and bearing clearance, Mech.Syst. Sig. Process. 85 (2017) 445–467.
[27] Y. Chen, T. Yang, S. Choi, Dynamic analysis of a double-helical geared rotor system with oil-film bearing, Aircr. Eng. Aerosp. Tec. 92 (2020) 653–662.
[28] H. Ocak, K.A. Loparo, F.M. Discenzo, Online tracking of bearing wear using wavelet packet decomposition and probabilistic modeling: a method for bearing prognostics, J. Sound Vib. 302 (2007) 951–961.
[29] P. Zmarzły, Influence of the internal clearance of ball bearings on the vibration level, in: 24th International Conference Engineering Mechanics 2018, Svratka, Czech Republic, May 14–17, 2018, pp: 961–964.
[30] A. Georgiadis, X. Gong, N. Meier, Vibration analysis based on the spectrum kurtosis for adjustment and monitoring of ball bearing radial clearance, in: MATEC Web of Conferences 211, 2018.
[31] N. Meier, B. Ambrożkiewicz, A. Georgiadis, Verification of measuring the bearing clearance using kurtosis, recurrences and neural networks and comparison of these approaches, in: Proceedings of the IEEE SENSORS, IEEE, 2019, pp: 1–4.
[32] S. Kumar, D. Goyal, R.K. Dang, Condition based maintenance of bearings and gears for fault detection-A review, Materials Today Proceed. 5(2) (2018) 6128–6137.
[33] R.B. Randall, Detection and diagnosis of incipient bearing failure in helicopter gearboxes, Eng. Fail. Anal. 11(2) (2004) 177–190.
[34] R. Zhang , J.X. Gu, F. Gu, Gear Wear Process Monitoring Using a Sideband Estimator Based on Modulation Signal Bispectrum, Appl. Sci. 7 (3) (2017) 274.
[35] R. Zhang, F. Gu, H. Mansaf, Gear wear monitoring by modulation signal bispectrum based on motor current signal analysis, Mech. Syst. Sig. Process. 94 (2017) 202–213.
[36] X. Sun, R. Zhang, K. Lu, Monitoring of gear wear progressions based on a modulation signal bispectrum analysis of vibration, in: the sixteenth international conference on condition monitoring and asset management (CM 2019), BINDT, 2019. https://www.bindt.org/events/CM2019/124-abstract/
[37] J. Wang, M. Xu, C. Zhang, Online Bearing Clearance Monitoring Based on an Accurate Vibration Analysis, Energies, 13 (2020) 389.
[38] S.R. Schmid, B.J. Hamrock and B.O. Jacobson, Fundamentals of Machine Elements, SI Version, CRC Press, Boca Raton, 2014.
[39] I. Rehab, The Optimization of Vibration of Data Analysis for the Detection and Diagnosis of Incipient Faults in Rolling Bearings. University of Huddersfield, 2017, Feb.
[40] D.J. Inman, Engineering Vibration, Prentice Hall, 1994.
[41] X. Tian, Dynamic simulation for system response of gearbox including localized gear faults. University of Alberta, 2004
[42] X. Liang, M.J. Zuo, T.H. Patel, Evaluating the time-varying mesh stiffness of a planetary gear set using the potential energy method, Proceed. Inst. Mech. Eng., Part C: J. Mech. Eng. Science. 228(3) (2014) 535-547.
[43] C. Chen, T. Xu, G. Wang, Railway turnout system RUL prediction based on feature fusion and genetic programming. Measurement 2020; 151: 107162.
[44] Zhang B, Zhang L, Xu J. Degradation feature selection for remaining useful life prediction of rolling element bearings. Qual Reliab Eng Int 2016; 32: 547-554.